International Journal of Precision Engineering and Manufacturing-Green Technology (2025) 12:409–430
https://doi.org/10.1007/s40684-024-00655-3

Online ISSN 2198-0810
Print ISSN 2288-6206

REGULAR PAPER

Machining and Sustainability Performance Comparison for the Milling Process of Al6082 Alloy Under Various Minimum Quantity Lubrication Conditions

Yusuf Furkan Yapan[1] · Kerim Türkeli[1] · Uğur Emiroğlu[2] · Erkan Bahçe[3] · Alper Uysal[1]

Received: 29 April 2024 / Revised: 30 July 2024 / Accepted: 6 August 2024 / Published online: 17 August 2024

Abstract

Aluminum 6082 alloys are commonly utilized in significant industries because of their unique characteristics. However, they exhibit poor machinability as a result of their high ductility, high thermal expansion coefficient, and tendency to built-up edge formation. Considering the alloy's widespread usage, the difficulty of machining it raises sustainability concerns. For this reason, although minimum quantity lubrication (MQL) methods using various nanoparticle-added nanofluids have been used to enhance machinability, the use of graphene nanoparticles (GNP) has been ignored. Furthermore, there has been a lack of sustainability assessment and optimization. In the presented study, MQL methods using various GNP-added nanofluid (N-MQL) was used for the first time in the milling of Al6082 alloy, and its machining responses (cutting temperature, cutting force, feed force, surface roughness, and chip morphology) and sustainability indicators (carbon emission and total machining cost) were determined and compared with dry-cutting and pure MQL utilizing vegetable cutting oil. The utilization of the N-MQL, as opposed to the dry-cutting with appropriate cutting parameters, resulted in improvements of 50.6% in cutting force, 65.4% in feed force, 50.6% in cutting temperature, 33.2% in chip width, 15.3% in chip length, 67.3% in surface roughness, 21.5% in carbon emissions, and 52.6% in machining cost. Finally, applying multi-objective optimization using NSGA-II (non-dominant sequencing genetic algorithm II) and the multi-criteria decision-making method using VIKOR, optimum process parameters were determined in terms of sustainability-weighed carbon emissions and total machining cost. From the sustainability-based optimization results, it was determined that the cutting speed should be selected between 36 and 40 m/min, the feed should be selected between 0.14 and 0.18 mm/rev, and the N-MQL method should be used. Using the N-MQL method at above-average cutting speeds and feed values are the most sustainable machining parameters and condition for milling of Al6082.

Keywords Graphene nanofluid · Minimum quantity lubrication · Machining responses · Sustainability analysis

List of Symbols

a_p	Depth of cut
Al	Aluminium
Al_2O_3	Aluminium oxide
C	Correction factor
CC	Cutting condition
CNT	Carbon nanotube
CE	Total carbon emission
CE_{el}	Carbon emission resulting from the electricity
CE_{tool}	Carbon emission resulting from the cutting tool
$CE_{material}$	Carbon emission resulting from the material
CE_{chip}	Carbon emission resulting from the chip
CE_c/l	Carbon emission resulting from the cooling/lubricating
CEF_{el}	Electricity carbon emission factor
CEF_{tool}	Tool carbon emission factor
$CEF_{material}$	Material carbon emission factor
CEF_{chip}	Chip carbon emission factor

✉ Yusuf Furkan Yapan
yapan@yildiz.edu.tr

[1] Department of Mechanical Engineering, Yildiz Technical University, 34349 Istanbul, Turkey

[2] Department of Motor Vehicles and Transportation Technologies, Kastamonu University, 37000 Kastamonu, Turkey

[3] Department of Mechanical Engineering, Inonu University, 44280 Malatya, Turkey

CEF_c/l	Cooling/lubricating carbon emission factor
Cu	Copper
E_{total}	Total energy
Fe	Iron
F_c	Cutting force
F_f	Feed force
f	Feed value
Ga	Gallium
HSS	High speed steel
H	Hardness of workpiece
K	Cutting tool energy consumption constant
MC	Total machining cost
$MC_{milling}$	Costs resulting from the milling process
MC_{energy}	Costs resulting from the energy consumption
MC_{fluid}	Costs resulting from the cutting fluid consumption
MC_{tool}	Costs resulting from the cutting tool
$MC_{environment}$	Costs resulting from the environmental impact
Mg	Magnesium
Mn	Manganese
MQL	Minimum quantity lubrication
MoS_2	Molybdenum disulfide
MRR	Maerial removal rate
GNP	Graphene nanoparticle
$N\text{-}MQL$	Minimum quantity lubrication with nanofluid
$NSGA\text{-}II$	Non-dominated sorting genetic algorithm II
μ_{nf}	Effective viscosity of the nanofluid
μ_{bf}	Effective viscosity of the base fluid
φ_e	Effective volume fraction
φ	Percent volume fraction
r	Radius of the nanoparticle
h	Thickness of the nanoparticle
K_b	Boltzman constant
ρ_P	Density of nanoparticle
d_p	Diameter of nanoparticle
P_c	Cutting power
R_a	Surface roughness
SDS	Sodium dodecyl sulphate
SEM	Scanning electron microscope
Si	Silicon
SiC	Silicon carbide
SiO_2	Silicon dioxide
t_c	Cutting time
T_{tool}	Tool life
T_c	Cutting temperature
Q	MQL flow rate
ρ	Material density
V	Vanadium
V_c	Cutting speed
W_{tool}	Cutting tool weight
Zr	Zirconium

1 Introduction

Aluminum alloys are extensively utilized in aerospace [1], automotive [2], marine [3], and construction applications [4] owing to their distinctive amalgamation of characteristics, including favorable corrosion resistance and strength/weight ratio [5, 6]. Despite these advantages, it has been reported that there are difficulties in machining aluminum alloys due to high ductility, the high thermal expansion coefficient, the built-up edge, and the built-up layer [7, 8]. In addition, because of the challenges and widespread applications, sustainability concerns arise in machining aluminum alloys. For this reason, there is a requirement for advanced machining techniques that will enhance the sustainability [9, 10] and efficacy of machining [11, 12].

Experimental results indicate that the minimum quantity lubrication (MQL) method, as opposed to the conventional fluid cutting method, can enhance machining performance and sustainability [13, 14]. However, in the machining of materials that are difficult to cut, such as aluminum alloys, MQL parameters must be adjusted appropriately in order for the aerosol droplets to reach the cutting zone effectively [15]. Davim et al. [16] stated that choosing appropriate MQL parameters in drilling AA1050 alloy would exhibit similar machining performance to conventional flood cutting, and Nandi and Davim [17] determined the optimum parameters using a fuzzy logic algorithm. In high-speed milling of an A356 aluminum alloy, Kishawy et al. [18] examined the cutting force (F_c) under dry, flood, and MQL conditions, and the F_c were reduced under the MQL cutting condition. Tosun and Huseyinoglu [19] investigated the effect of surface roughness (R_a) and burr formation of wet and MQL conditions in the face milling of AA7075-T6. The effect of the MQL method on R_a in end milling of 6061 alloys was investigated by Joshua et al. [20] by comparing it with dry-cutting. The results demonstrate that, in addition to being environmentally benign, machining under the MQL environment lowered the R_a value to roughly 20%, resulting in a better surface quality. Khettabi et al. [21] investigated the machining performance, F_c, particle emission, and R_a in high-speed milling 7075, 6061, and 2024 aluminum alloys under dry and MQL conditions. It has been stated that MQL conditions give better results at low cutting speed (V_c) values. Conger et al. [22] investigated the effect of using a single or double MQL nozzle in the milling of 6061 alloys. Dual nozzles have reduced F_c, feed force (F_f), and R_a. Zhu et al. [23] studied the optimization of the MQL distance by considering the F_c and R_a s in the milling of the aluminum 2A12 alloy. Imthiyas et al. [24] reduced the R_a by 22.4%

compared to dry-cutting by using the MQL method in the milling of Al6063 alloys.

However, since the heat generated during the cutting of materials that are challenging to process can't be completely eliminated by the MQL method [25], the cooling capacity of the fluid used in the MQL method must be increased. Therefore, the primary focus of research to improve MQL performance has lately shifted to nanofluid-assisted MQL (N-MQL) applications [26]. In the N-MQL method, parameters must be selected because nanoparticle concentration [27], particle size [28], and homogeneous distribution of nanoparticles in the fluid affect the machining performance. Various studies have been carried out on the effective machinig of aluminum alloys with the N-MQL method. For example, Rahmati et al. [29] used MoS_2 N-MQL to evaluate the surface quality of Al6061-T6 aluminum alloy during milling. The results showed that the MoS_2 N-MQL method could be an alternative to obtaining good surface quality. Najiha ve Rahman [30] investigated the effects of water-based TiO_2 nanofluid and wet cutting on tool wear mechanisms in the end milling of AA6061 alloy. The water-based nanofluid MQL's main advantage may be seen in the edges' intact shape, which exhibits minimal chipping and edge breakage. Yuan et al. [31] investigated the effect of N-MQL conditions obtained by adding copper, silicon carbide, and diamond nanoparticles to three different vegetable oils, soybean, canola, and natural77, on the machining performance in end milling of 7050 alloys. The results demonstrate that natural77 oil-based diamond nanofluids perform the lowest R_a, and canola oil-based diamond nanofluids present the lowest F_c compared to dry machining conditions, respectively, with 10.71 and 14.92% reductions. Kulkarni et al. [32] investigated the effects of dry, MQL, and copper-coated aluminum oxide N-MQL conditions on the R_a and cutting temperature (T_c) in the milling of Al7075-T6 alloy. N-MQL conditions lowered the T_c more, while MQL conditions resulted in lower R_a. Raza et al. [33] investigated the effects of dry, MQL, and Al_2O_3 N-MQL conditions on R_a and material removal rate (*MRR*) for Al6082-T6. As a result, MQL and N-MQL reduced R_a by 30% and 46%, respectively, compared to dry conditions. Also, a negligible effect of cutting conditions is observed for the *MRR*. Gao et al. [34] investigated the effect of Al_2O_3, MoS_2, SiO_2, CNTs, SiC, and Graphite N-MQL conditions on the F_c and chip morphologies in milling Al7075 alloy. The lowest F_c was obtained in MoS_2 N-MQL conditions, and it was determined that the machined surface and chip surface morphology were better in SiO_2, Al_2O_3, and SiC N-MQL conditions. Safiei et al. [35] used SiO_2–Al_2O_3–ZrO_2 hybrid N-MQL for end-milling aluminum 6061-T6 alloy, reducing the F_c. Bhavsar and Kulkarni [36] used SiO_2 N-MQL to end-mill the AA6063 alloy, improving the surface quality. MQL and 9:1 ratio Al_2O_3/Graphene hybrid N-MQL were used in the milling of 6061 aluminum alloy by Tiwari et al. [37]. As a result, the hybrid N-MQL condition provided a 15.98% reduction in F_c compared to the MQL condition.

As can be seen in the paragraph above, although studies have been presented to improve the cutting performance in the milling of aluminum alloys with the N-MQL method using various nanoparticles, a study using the nanographene (GNP) particle-reinforced N-MQL method has not yet attracted attention. GNP, which has superior mechanical properties, can protect the contact surface in friction when used as a lubricant addition. Moreover, the excellent thermal conductivity of graphene nanosheets can further improve the performance of the lubricating film by lowering the local temperature in the friction zone of the materials rubbing in contact. The weak interlayer interaction also helps enhance its tribological characteristics [38–40]. Due to these unique properties, the effect of the GNP-reinforced N-MQL method on various machining methods and diverse materials except aluminum alloys has been studied. For example, Park et al. [41] reported reduced tool wear in milling AISI 1045 steel using N-MQL doped with 0.1% by weight GNP. Uysal [42] determined that the milling of AISI 430 ferritic stainless steel reduces tool wear when using 2% by weight GNP N-MQL and a flow rate of 40 ml/h MQL. It was presented in the study by Pavan et al. [43] that the surface quality was increased in the grinding of Inconel 718 alloy with 0.3% by weight GNP N-MQL method. Uysal [44] obtained the least and smallest burr forms with minimum T_c by using the 0.5% by weight GNP N-MQL method in milling AISI 430 alloy. Huang et al. [45] used wt. 1% GNP reinforced N-MQL in micro-milling of SKD11 die steel and reduced the F_c by 12.9% compared to the pure MQL method. Pal et al. [46] used the N-MQL method containing 1.5% by weight GNP to drill AISI 321 stainless steel, and compared to the pure MQL method, the F_f, torque, R_a, and coefficient of friction decreased by 27.4%, 64.9%, 33.8%, and 51.7%, respectively. Sahoo and Datta [47] reduced the F_c, by 70% compared to dry-cutting by using the N-MQL method with 0.1% by weight GNP-reinforced Jatropha oil in the turning of Ti-6Al-4V alloy. It was reported by Baldin et al. [48] that adding 0.1% by weight GNP sheets to vegetable-based cutting fluid effectively increased the lubricating properties. Danish et al. [49] investigated the milling performance of Inconel 718 alloy by the MQL method by adding 0.7% by weight GNP to sunflower oil. As a result, it reduced R_a by 49%, F_c by 25%, T_c by 31%, and tool wear by 20% compared to dry-cutting.

The comprehensive literature review demonstrates that there remains a great deal of ambiguity regarding the machining response of the MQL method when utilizing graphene-reinforced nanofluid (N-MQL) for the machining of aluminum alloys, which are classified as hard-to-cut materials because of their high ductility, high thermal expansion coefficient, and chip accumulation. In addition, the effect of the graphene N-MQL method on sustainability indicators such as carbon emissions (*CE*) and total machining costs (*MC*) has not been investigated. In the presented study, the graphene-reinforced N-MQL method was used for the first time in milling Al6082 alloy and the effect of the method on machining responses (cutting temperature (T_c), cutting force (F_c), feed force (F_f), surface roughness (R_a), and chip morphology) and sustainability indicators (*CE* and *MC*) was investigated. Then, by applying multi-objective optimization (*MOOP*) using NSGA-II (non-dominant sequencing genetic algorithm II) and multi-criteria decision making method (*MCDM*) using VIKOR, optimum process parameters were determined in terms of sustainability weighted on *CE* and *MC*.

2 Materials and Method

2.1 Preparation of Nanofluids

It is known that nanoparticles can be used effectively as additives to increase the lubricating ability of vegetable oils [50]. In this study, nanoparticle-added cutting fluid was prepared for the MQL method using graphene nanoparticle (GNP)-added nanofluid (N-MQL). The GNP brand utilized in the study is GRAFEN®-NG5. Technical details and scanning electron microscope (SEM) image of this GNP can be seen in Table 1.

The schematic representation of the stages involved in the preparation of nanofluids is depicted in Fig. 1. Due to the authors' previous literature experience and knowledge, the weight percentage of nanoparticles was chosen as 0.8% [51]. The GNPs underwent a drying process for a duration of 120 min at a temperature of 120 °C using a thermal brand G11420SD model oven in order to eliminate the moisture present within them. In order to prepare a GNP-added nanofluid using desiccated nanoparticles, a concentration of 0.8% by weight of GNP was introduced into a commercially available vegetable cutting fluid. A precision balance, the Radwag PS 510.R1, was used to weigh the nanoparticles. The cutting fluid employed in the conducted research is Eraoil KT/2000, a commercially available cutting fluid derived from vegetable sources. The vegetable-based cutting oil has a reddish-orange color, a density of 0.85 g/cm^3 at 20 °C. In order to enhance the uniformity of the nanofluid containing GNPs and extend the duration of sedimentation, sodium dodecyl sulphate (SDS) was introduced into the mixture as a surfactant, at a concentration of 0.1% relative to the weight of GNPs. The prepared mixes were subjected to mixing at a speed of 5000 revolutions per minute (rpm) for a duration of 1 h, utilizing the Daihan WiseTis HG-15D digital homogenizer. Afterwards, the prepared nanofluid was transferred to the MQL system.

Table 1 Technical specifications and SEM images of GNP

Properties	GNP	SEM image
Color	Black	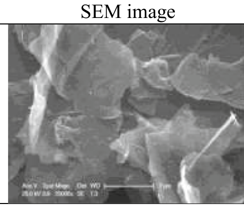
Purity (%)	99	
Thermal conductivity (W/mK)	~5000	
Surface area (m^2/g)	120-150	
Density (g/cm^3)	2	
Diameter (µm)	5-10	
Thickness (nm)	5-8	

The viscosity of the commercial vegetable cutting oil (base cutting fluid) in the presented study is 11 cst at 20 °C room temperature, and the viscosity value of the vegetable cutting fluid containing 0.8% GNP nanoparticles by weight was calculated using the empirical equations reported by Klazly and Bognar [52]. The ratio of the effective viscosity of the nanofluid (μ_{nf}) to the effective viscosity of the base fluid (μ_{bf}) was determined with the help of the relation given in Eq. (1).

$$\frac{\mu_{nf}}{\mu_{bf}} = 1 + 9.4974 * \varphi_e + 77.811 * \varphi_e^2 + 0.9514 * \varphi_e^3 + \frac{\sqrt{\frac{18 * K_b * T * \rho_P}{\pi}}}{39.6231 * \sqrt[3]{\frac{\pi}{\varphi_p}} * C * \sqrt{d_p}} \quad (1)$$

Here φ_e is the effective volume fraction. The effective volume fraction was calculated with the help of Eq. (2) and depends on the percent volume fraction (φ), radius (r) and thickness (h) of the nanoparticle. K_b represents the boltzman constant and its value is 1.380649×10^{-23}. T is the room temperature in kelvins. C is the correction factor and is assumed to be a function of φ and T. ρ_P and d_p represent the density and diameter of graphene nanoparticle, respectively, and their values are presented in Table 1.

$$\varphi_e = \varphi * \left(1 + \frac{h}{r}\right) \quad (2)$$

Using the relevant equations, the viscosity value of the vegetable-based cutting fluid containing 0.8% graphene by weight was calculated as 13.09 cst at room temperature. It is known that nanoparticles added to vegetable oil affect the stability and lubrication abilities of nanofluids by increasing the viscosity values of the fluid [53]. Adding nanoparticles to the lubricant increases the density and viscosity of the fluid while also increasing the thermal conductivity of the lubricant [54]. In addition, increasing the viscosity value is beneficial in keeping the lubricant in the cutting zone [55].

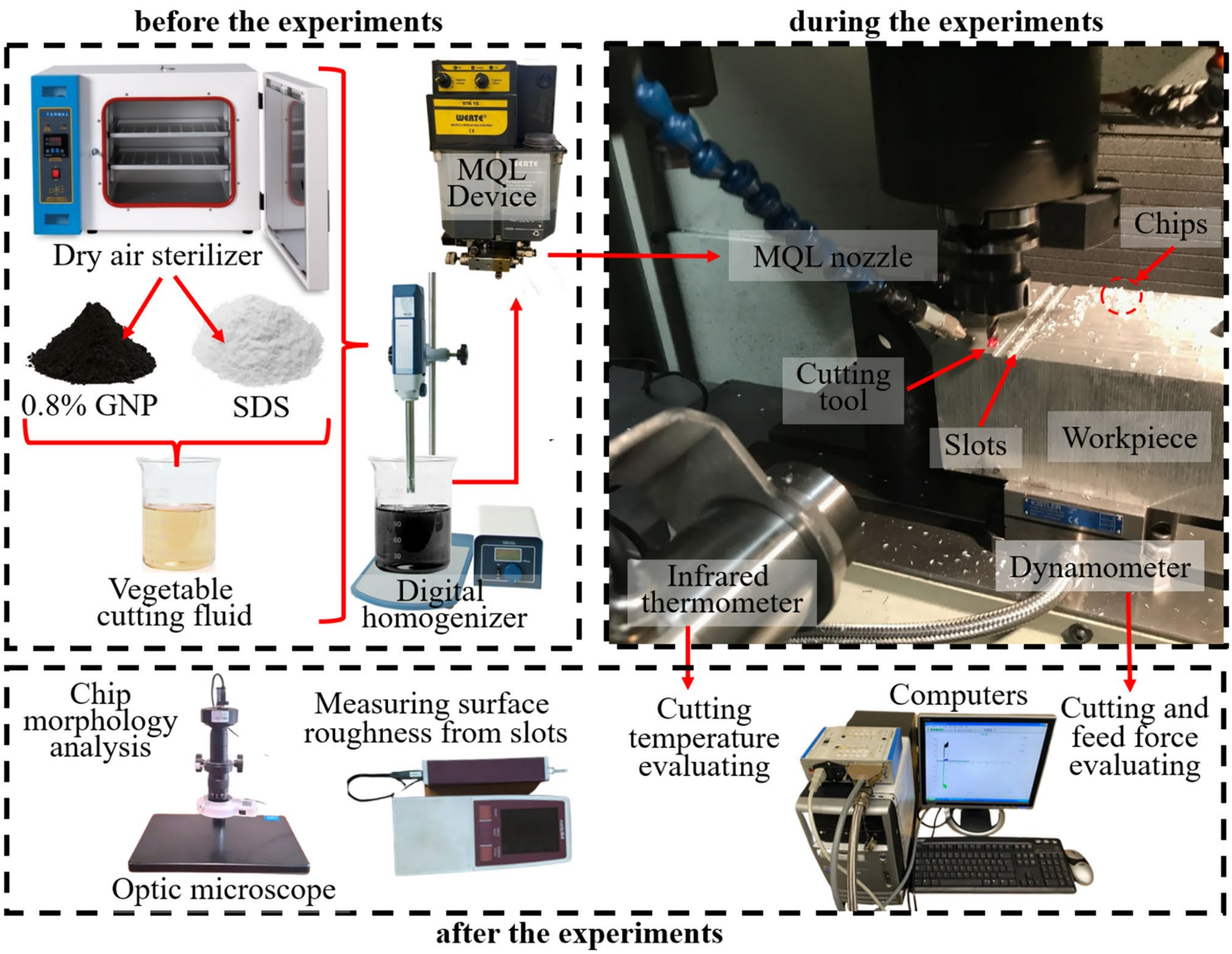

Fig. 1 Experimental setup

Table 2 Mechanical properties of the workpiece

Yield strength	Tensile strength	Ductility	Hardness
230 MPa	400 MPa	6–8%	90 HB

2.2 Workpiece Material, Machine Tools, and Equipment

In experimental studies, Al6082 aluminum alloy was used as a workpiece. Al6082 is an aluminum alloy that belongs to the 6000 series. It is a heat-treatable alloy with good mechanical properties, corrosion resistance, and weldability [5, 6]. The mechanical properties and chemical composition of the workpiece are given in Tables 2 and 3, respectively.

The studies were carried out using the First MCV-300 CNC milling machine of Taiwan origin and the experimental setup is given in Fig. 1. All experiments were performed with the 8 mm diameter uncoated HSS cutting tool end mill with four cutting edges.

The Kistler brand 9257BA model dynamometer and Kistler brand 5233A model control panel were used to measure the forces during the milling tests. The dynamometer used measures forces in three global axes, and cutting force (F_c) and feed force (F_f) are presented in the study. The measured force values were processed in a computer environment via DynoWare software.

Table 3 Chemical composition of the workpiece

Element	Al	Si	Mg	Mn	Fe	Ga	V	Zr	Cu
Wt%	97.59	1.085	0.979	0.502	0.114	0.0098	0.0096	0.0023	0.0005

The cutting temperature (T_c) was measured in the studies using dual-laser Optris CTlaser non-contact temperature measuring equipment, commonly referred to as a pyrometer. By directing the lasers toward the cutting edge of the cutting tool, the temperature of the cutting zone was ascertained. Compact Connect software was used on the computer to process the temperature measurement device's data.

The surface roughness (R_a) of the samples processed following the milling procedures was measured using a Mitutoyo Surftest SJ-210 model R_a measurement device. Measurements were made 15 times in total, with 5 repetitions, from three regions: the entrance, middle, and exit of the machined slot, and the average of the results is presented.

Images of chips generated during the milling process, which were captured using an SOIF XLB45-B3 digital stereo microscope equipped with a 3 MP MD30 camera and MShot software. Their width and length were calculated in ImageJ software.

The experiments were carried out using the Werte DKN 25 model MQL system. To prevent the nanoparticles from clumping in the MQL device, blocking the device pipes, and delivering the healthy nanofluid to the cutting zone, a propeller system driven by an electric motor and adjustable speed was used in the MQL device. The MQL device operated at a pressure of 5 bar and had a flow rate of 21 ml/h. The MQL device's nozzle, which has a 1 mm tip radius, is adjusted to a constant 50° angle and 20 mm distance for every experiment. The authors' prior expertise and familiarity with relevant MQL parameters proved advantageous in the process of determining MQL settings [56, 57].

Table 4 Milling experiment plan

Sample no.	*CC*	V_c (m/min)	f (mm/rev)	a_p (mm)
S1	Dry	30	0.1	2
S2	Dry	30	0.15	
S3	Dry	30	0.2	
S4	Dry	35	0.1	
S5	Dry	35	0.15	
S6	Dry	35	0.2	
S7	Dry	40	0.1	
S8	Dry	40	0.15	
S9	Dry	40	0.2	
S10	MQL	30	0.1	
S11	MQL	30	0.15	
S12	MQL	30	0.2	
S13	MQL	35	0.1	
S14	MQL	35	0.15	
S15	MQL	35	0.2	
S16	MQL	40	0.1	
S17	MQL	40	0.15	
S18	MQL	40	0.2	
S19	N-MQL	30	0.1	
S20	N-MQL	30	0.15	
S21	N-MQL	30	0.2	
S22	N-MQL	35	0.1	
S23	N-MQL	35	0.15	
S24	N-MQL	35	0.2	
S25	N-MQL	40	0.1	
S26	N-MQL	40	0.15	
S27	N-MQL	40	0.2	

2.3 Desing of Milling Experiments

In the sustainable milling experiments, three different cutting conditions (*CC*), including dry, MQL with vegetable-based cutting fluid, and N-MQL with vegetable-based cutting fluid containing 0.8% GNP by weight, were used, together with three different cutting speed (V_c) values of 30, 35, and 40 m/min and feed (f) values of 0.1, 0.15, and 0.2 mm/rev. A full factorial experiment plan was designed with 27 experiments, and these experiments are given in Table 4. The depth of cut (a_p) of 2 mm was maintained steadily in all experiments. The experiments were run three times to guarantee the accuracy of the findings. Since the deviation between the results was less than 5% and the average results were presented.

3 Results and Discussion

In this section, the machining responses were evaluated in terms of cutting temperature (T_c), cutting force (F_c), feed force (F_f), surface roughness (R_a), and chip morphologies based on various cutting conditions (*CC*) and cutting parameters such as cutting speed (V_c) and feed (f). Then, a sustainability assessment was performed regarding total carbon emissions (*CE*) and total machining costs (*MC*). The all results obtained are given in the Table 5. Coloring was performed from green to red from minimum result to maximum result. After all this, the optimum process parameters in terms of sustainable machining were determined by multi-objective optimization and multi-criteria decision-making based on *CE* and *C*.

3.1 Machining Responses

3.1.1 Cutting Temperature (T_c)

The deformation energy applied to the workpiece during chip formation is converted into heat [58]. This energy is spent in four works: (i) cutting the material in the primary cutting zone, (ii) plastically deforming the chip in the second cutting zone, (iii) conveying the newly formed chip to the rake surface, (iv) friction in the tertiary shear zone [59,

Table 5 Experimental and sustainability analysis results

No	*CC*	V_c (m/min)	*f* (mm/rev)	F_c (N)	F_f (N)	T_c (°C)	R_a (µm)	*CE* ($kgCO_2$)	*MC* ($)
1	Dry	30	0.1	346.89	143.46	44.27	1.68	0.5806	4.61441
2	Dry	30	0.15	440.55	168.72	48.59	2.4	0.53673	3.69274
3	Dry	30	0.2	490.71	202.41	50.48	3.4	0.51257	3.19824
4	Dry	35	0.1	323.40	133.24	47.20	2.25	0.56367	4.24879
5	Dry	35	0.15	430.62	155.60	50.10	2.81	0.5242	3.42895
6	Dry	35	0.2	482.12	190.06	55.30	3.93	0.50243	2.9887
7	Dry	40	0.1	300.99	125.00	51.08	2.88	0.55035	3.96516
8	Dry	40	0.15	422.50	150.00	52.54	3.252	0.51436	3.22411
9	Dry	40	0.2	475.28	183.93	64.51	4.21583	0.49446	2.82589
10	MQL	30	0.1	278.10	97.31	34.30	1.5256	0.5618	4.27018
11	MQL	30	0.15	361.11	118.99	40.20	2.329	0.5225	3.43692
12	MQL	30	0.2	488.12	185.11	42.10	3.2614	0.50107	2.99104
13	MQL	35	0.1	274.30	85.56	36.40	1.6837	0.54663	3.93862
14	MQL	35	0.15	351.36	112.71	42.60	2.533	0.51126	3.19844
15	MQL	35	0.2	467.96	149.29	45.30	3.746	0.49197	2.80201
16	MQL	40	0.1	252.10	75.39	39.60	1.8885	0.53466	3.68176
17	MQL	40	0.15	340.87	105.00	44.60	2.74	0.50243	3.01351
18	MQL	40	0.2	426.53	123.07	47.40	3.87	0.48478	2.65531
19	N-MQL	30	0.1	277.55	97.00	31.88	1.379	0.50306	3.32248
20	N-MQL	30	0.15	359.74	114.97	34.85	1.771	0.47782	2.73298
21	N-MQL	30	0.2	435.36	169.09	38.48	2.326	0.46546	2.42099
22	N-MQL	35	0.1	264.28	79.00	33.20	1.5095	0.4936	3.08489
23	N-MQL	35	0.15	342.08	90.37	36.05	2.057	0.47177	2.56431
24	N-MQL	35	0.2	427.24	128.89	40.31	3.392	0.45987	2.2885
25	N-MQL	40	0.1	242.56	70.00	35.11	1.67275	0.48616	2.90186
26	N-MQL	40	0.15	337.25	80.00	38.32	2.584	0.46565	2.43423
27	N-MQL	40	0.2	418.98	120.00	42.20	3.682	0.45549	2.18623

60]. The heat generated at the interface between the cutting tool and the chip is the primary factor that controls the T_c at that location [51]. The T_c values obtained from the experiments are given in Fig. 2. In the figure, V_c values of 30, 35, and 40 m/min are divided into three sections, and the effect of milling conditions on T_c at different *f* values is shown. Increasing the V_c from 30 to 35 m/min increased the T_c by 5.5%, and increasing the V_c from 30 to 40 m/min increased the T_c by 12.1%. Similarly, increasing the *f* value from 0.1 to 0.15 mm/rev and from 0.1 mm/rev to 0.2 mm/rev increased the T_c by 9% and 17.1%, respectively. According to Safiei et al. [35], when milling 6061-T6 aluminum alloy, increasing the V_c and *f* leads to an increase in the T_c at the contact surface between the tool and workpiece. This is attributed to the accumulation of strain energy and friction resulting from the severe cutting parameters.

Additionally, the experimentally obtained T_c values were statistically analyzed in full quadratic fashion using the response surface method. Regression analysis was performed using Minitab statistical software to model response variables. The contribution rates of cutting parameters such as *CC*, V_c, and *f* to the T_c were determined to be 64.48%, 9.1%, and 19.25%, respectively. In addition, the interaction of the cutting parameters (CC^2, V_c^2, f^2, $CC*V_c$, $CC*f$, and V_c*f) with each other was determined since the method used is full quadratic. The most effective interactions here are CC^2 and $CC*V_c$, with contribution ratios of 2.94% and 1.12%, respectively.

The highest T_c was obtained using 40 m/min V_c and 0.2 mm/rev *f* value in dry-cutting. The absence of lubrication and high friction in dry cutting environments result in the highest T_c [13]. The lowest T_c was obtained under N-MQL lubricating conditions when a V_c of 30 m/min and a *f* value of 0.1 mm/rev were used. As a result, T_c was improved by 50.6%. The cutting fluids cool the chip and the workpiece and may even reduce the friction at the tool-workpiece and tool-chip interfaces [61]. Average T_c values for dry, MQL, and N-MQL were determined as 51.6 °C, 41.4 °C, and 36.7 °C, respectively. As expected from the literature, using vegetable-based lubricant in the MQL method reduced the T_c by 19.7% in the dry-cutting condition. The MQL method reduced the interface friction and somewhat removed the heat. On the other hand, the nanographene-reinforced N-MQL cutting condition decreased the T_c by 28.8% compared to the dry-cutting. A schematic representation of the lubrication mechanisms of

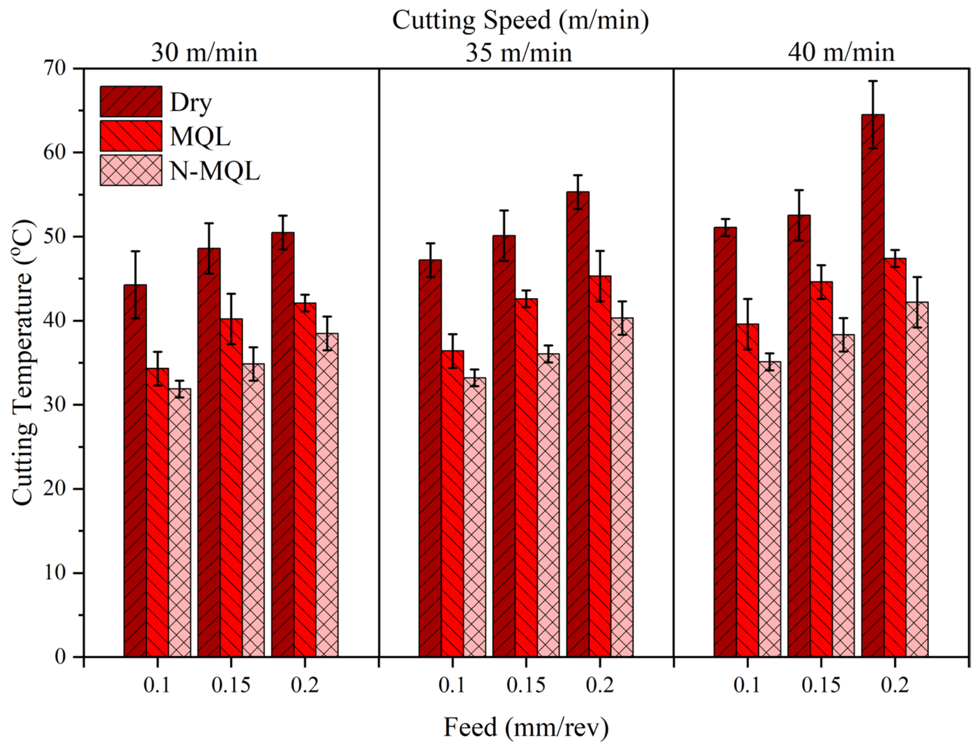

Fig. 2 Cutting temperature results

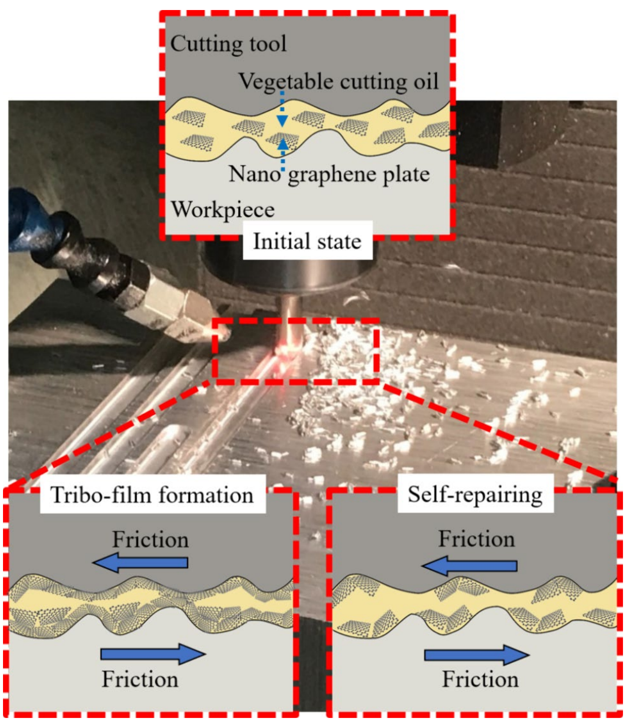

Fig. 3 A schematic representation of the lubrication mechanisms of graphene-reinforced N-MQL method; adapted and redrawn from [59, 61]

the graphene-reinforced N-MQL method is given in Fig. 3. As demonstrated in the initial state, graphene-reinforced vegetable cutting fluid can quickly enter the friction interface and prohibit between tool and workpiece friction surfaces due to their thin sheet structure, self-shear properties, high surface energy, and specific surface area [40, 62]. One of the lubrication mechanisms is a self-repairing mechanism known as the surface-mending effect [63]. The self-repair product reduces the contact between the mating surfaces by filling the micro-pits of the surfaces with nanoparticles [64]. Another lubrication mechanism is the tribo-film formation mechanism [49]. Tribo-film formation mechanism, the GNPs connect due to the high surface area/volume ratio and provide a thin protective layer along surfaces [64, 65]. These lubrication mechanisms reduce direct contact between the tool machining interface and minimize friction [40, 47]. The reduction of friction contributed to the decrease of the cutting temperature. In addition to lubrication mechanisms, graphene nanoparticles are well known to inherently transfer heat [66]. According to the data presented in Table 1, the thermal conductivity of graphene nanoparticles is approximately 5000 W/mK. The addition of graphene nanoparticles to the vegetable cutting fluid resulted in an enhancement of the fluid's thermal conductivity. It thus reduced the T_c for the N-MQL cutting condition by 7% compared to the pure MQL. The temperature reduces even more due to the fast removal of heat from the heated cutting zone made possible by graphene N-MQL's thermal conductivity.

3.1.2 Cutting Force (F_c) and Feed Force (F_f)

F_c is one of the primary chip removal process responses used to evaluate the machining performance. Several significant factors, including the cutting parameters, the machine tool's dynamics, the tool's and workpiece's material properties, MQL parameters, and the cutting fluid's tribological characteristics, affect the F_c [25, 50, 67, 68]. The F_c values obtained from the experiments are given in shades of red in Fig. 4. In the graphic, V_c values of 30, 35, and 40 m/min are divided into three sections, and the effect of cutting conditions on F_c at different f values is shown. Average F_c values for dry, MQL, and N-MQL cutting conditions were determined as 412.6 N, 345 N, and 306.1 N, respectively. In this case, the implementation of MQL and N-MQL conditions resulted in a decrease of the average F_c values by 12.7% and 16.4%, respectively, in comparison to the dry conditions. Also, increasing the f value from 0.1 to 0.2 mm/rev and decreasing the V_c from 40 to 30 m/min increased the F_c by 37.7% and 7.5%, respectively. Upon statistical analysis of the data, it was found that the f value, with a ratio of 81.45%, was the most effective parameter on the F_c. This was followed by the contribution rates of 12.5%, 2.5%, and 1.28% for CC, V_c, and CC^2.

The F_f values obtained from the experiments are given in shades of blue in Fig. 4. Average F_f values for dry, MQL, and N-MQL conditions were determined as 161.4, 116.9, and 105.5 N, respectively. The utilization of MQL and N-MQL resulted in a decrease of the average F_f values by 27.5% and 34.6%, respectively, in comparison to the dry-cutting. Also, increasing the f value from 0.1 to 0.2 mm/rev and decreasing the V_c from 40 to 30 m/min increased the F_f by 37.6% and 20.4%, respectively.

As a result, increasing the V_c from 30 to 40 m/min and reducing the f value from 0.2 to 0.1 mm/rev decreased the F_c and F_f, for all experiments. The highest F_c and F_f were obtained using 30 m/min V_c and 0.2 mm/rev f values in dry-cutting. In comparison, the lowest F_c and F_f were obtained under N-MQL cutting conditions when a V_c of 40 m/min and a f value of 0.1 mm/rev were utilized. As a result, 50.6% and 65.4% improvement was achieved in F_c and F_f, respectively. It was stated by Storchak et al. [69] that the contact at the chip tool interface increases as the V_c decreases. It is also known that the increase in f value causes an increase in friction at the tool-chip interface, thus increasing the T_c and F_c [70].

By combining cutting fluids and compressed air, a tiny droplet of aerosol is created in the MQL process. These aerosols are then fed at the tool-workpiece contact at a predetermined pressure. As a result, there is less friction at the tool-chip interface and the cutting forces are minimized as well as the chip is rapidly released [26, 71]. Using graphene-reinforced nanofluid MQL instead of conventional pure MQL reduced the F_c by 11.3% and F_f by 9.8%. The lubrication mechanisms' friction-reducing effect in Fig. 4 positively affects the cutting forces. According to Merchant [72] and Shi-Ramalingam [73] cutting force models, it is known that increasing friction increases the cutting force. Also, it was

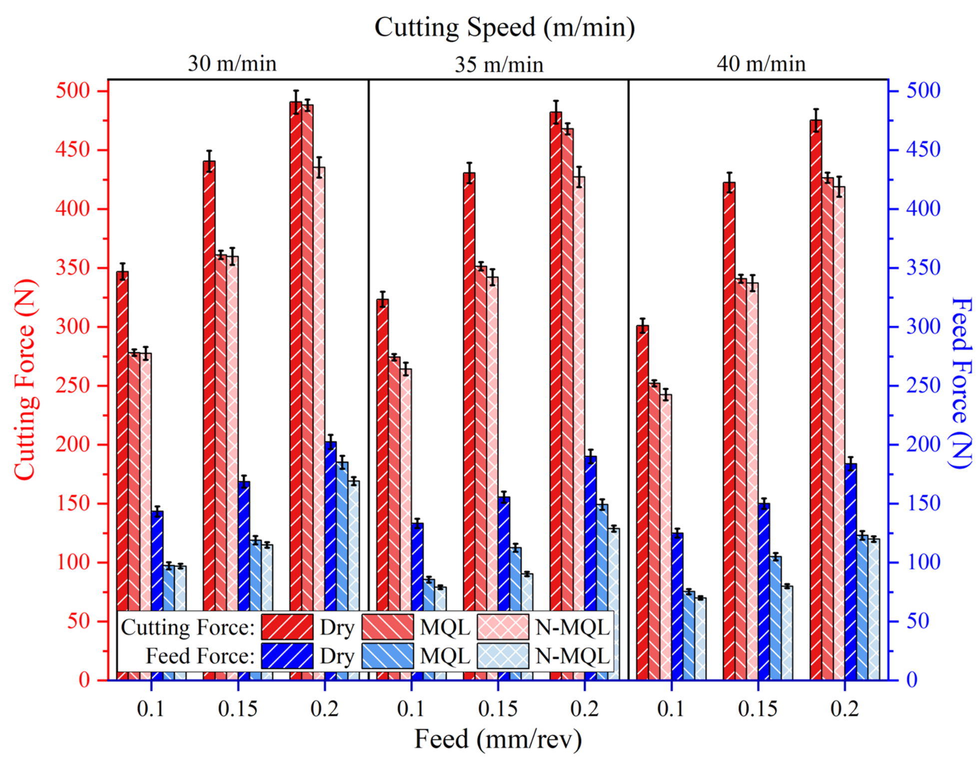

Fig. 4 Cutting and feed force results

stated by Tougguie et al. [51] that nanographene particles interact effectively with the cutting tool and workpiece due to their superior lubrication and superfine nanoscale structure, which would reduce friction and minimize the forces.

3.1.3 Surface Roughness (R_a)

The R_a values obtained from the experiments are given in Fig. 5. The figure illustrates how *CC* affects R_a values at various *f* values by dividing V_c values of 30, 35, and 40 m/min into three colouns.

The average R_a values for *CC* under dry, MQL, and N-MQL were measured as 3, 2.6, and 2.3 µm, respectively. The average R_a values were reduced under MQL and N-MQL than under dry-cutting by 12.1% and 24%, respectively. In a similar manner, Raza et al. [33] examined the impact of dry, MQL, and Al_2O_3 N-MQL on R_a for the Al6082-T6 alloy. Their findings revealed that MQL reduced Ra by 30%, while N-MQL reduced it by 46%, in comparison to dry-cutting. Also, reducing the V_c from 40 to 30 m/min and the *f* value from 0.2 to 0.1 mm/rev decreased the R_a by 33.4% and 48.2%, respectively. The analysis of R_a revealed that the *f* parameter had the highest impact, contributing 69.22% to the overall result. The V_c and *CC* parameters followed, with contribution ratios of 13.23% and 12.19%, respectively.

Under dry-cutting, the maximum R_a was achieved with a 40 m/min V_c and 0.2 mm/rev *f* value. In comparison, the N-MQL with a V_c of 30 m/min and a *f* value of 0.1 mm/rev obtained the lowest R_a. As a result, R_a was improved by 67.3%. The vegetable-based lubricant used in MQL cutting conditions reduced the friction coefficient and offered a good surface compared to dry cutting conditions. Similar results for milling in MQL conditions were reported by Uysal [74]. N-MQL cutting conditions, on the other hand, decreased the R_a by 11.5% compared to MQL conditions. Nanographene particles are recognized for their ability to decrease friction between the tool and the workpiece, resulting in improved machined surfaces [75]. The presence of nanoparticles in the micro-pit at the tool-workpiece interfaces leads to the production of a thin tribo-film, which in turn reduces direct contact between the tool and workpiece. This results in a decrease in friction and surface roughness [45, 76].

3.1.4 Chip Morphology

The notion of "chip morphology" refers to the complete geometry of a chip and is greatly influenced by the geometry of the tool and the mechanics of machining [77]. For a more thorough knowledge of the influence on the machining responses, it is essential to examine the chip formations during milling. Chip formation is influenced by the material of the workpiece, cutting parameters, and the rake angle of the tool [78]. To characterize the morphologies of the chips, both macro and micro studies are conducted on them [79]. In the work that is being given, the macro level analysis of chip morphologies was conducted. For this purpose, samples were collected from the chips obtained as a result of 27 tests.

Fig. 5 Surface roughness results

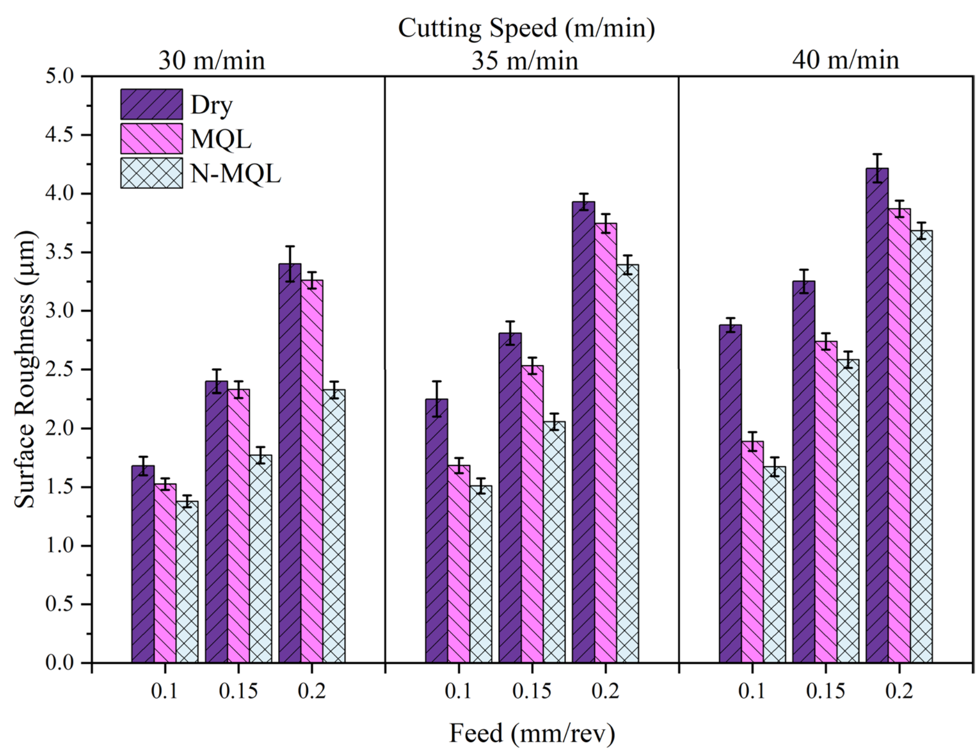

They were then examined under a microscope according to their experimental numbers. Images of chips generated during the milling process were obtained using a SOIF XLB45-B3 digital stereo microscope, a 3 MP MD30 camera, and MShot software. Chip images for dry, MQL, and N-MQL cutting conditions are given in Fig. 6. Their width and length were calculated in ImageJ software.

As can be seen from the figures, chips formed during milling are short tubular chips. Although the effect of V_c and f values is not obvious as a result of measuring chip dimensions, the effect of cutting conditions is clearly seen. Average chip length and width for dry cutting conditions were 1.20 mm and 0.52 mm, respectively; average chip length and width for MQL cutting conditions were 1.05 mm and 0.48 mm, respectively; average chip length and width for N-MQL cutting conditions were measured as 1.02 mm and 0.35 mm, respectively. MQL cutting conditions reduced chip length and width by 12.6% and 8.6%, respectively, compared to dry conditions, while N-MQL cutting conditions reduced chip length and width by 15.3% and 33.2%. Cutting fluids have the ability to distribute heat generated by shear and friction heating during the flow of chips and the deformation of materials. Additionally, they can facilitate the fragmentation of chips into smaller pieces, making it easier to efficiently evacuate and dispose of them [80]. Therefore, more minor chips were obtained in MQL and N-MQL compared to dry cutting conditions. N-MQL reduced chip length and width by 3.09% and 26.9%, respectively, compared to MQL conditions. It is widely acknowledged that graphene nanoparticles have a high heat conductivity by nature [81]. The temperature decreases more as a result of the rapid removal of heat from the heated cutting zone caused by graphene N-MQL's high thermal conductivity. Because of the material's embrittlement, this condition caused the formation of the lowest-sized chips. In comparison to N-MQL conditions, a less efficient chip was formed since MQL conditions were unable to demonstrate the intended performance in heat removal.

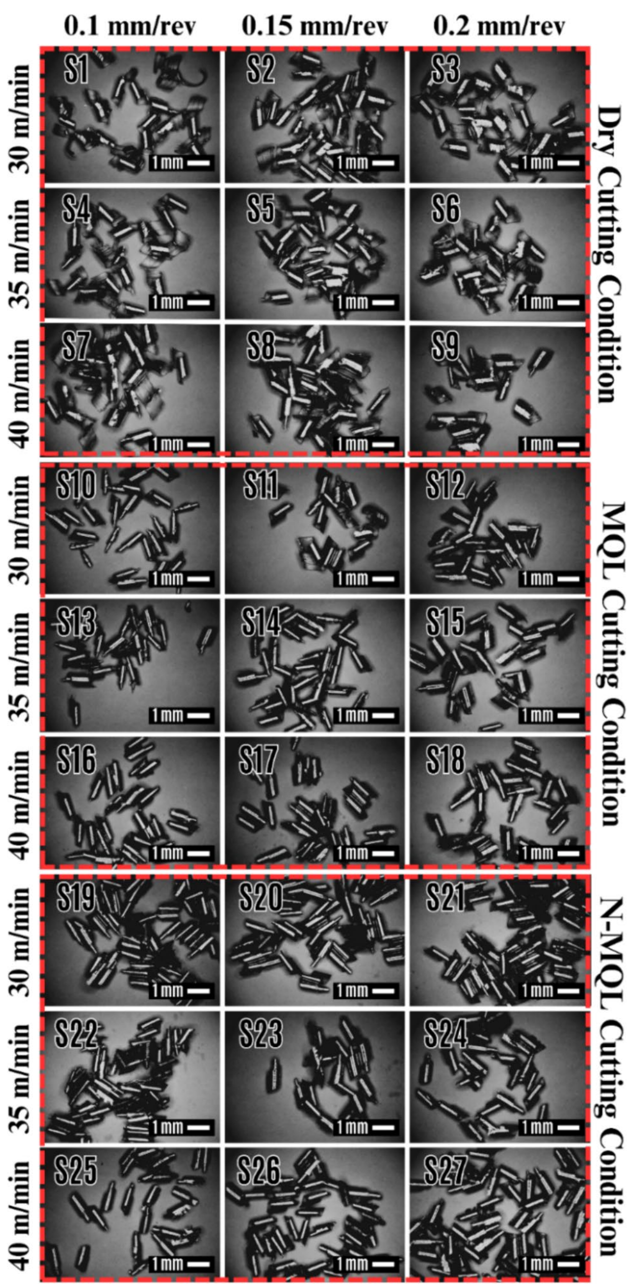

Fig. 6 Chip morphologies for dry, MQL, and N-MQL milling conditions

3.2 Assessment of Sustainability

As seen in Fig. 7, the presented study used two leading sustainability indicators to assess sustainability: total carbon emissions (*CE*) and total machining cost (*MC*).

3.2.1 Total Carbon Emissions (*CE*)

The mitigation of climate change impacts and the establishment of a sustainable future necessitate the significance of minimizing *CE* in manufacturing industries. Machining is the dominant production process as a primary and secondary

Fig. 7 Two leading machining sustainability indicators

process within the manufacturing industry, accounting for the highest business volume at a rate of 70%. Therefore, sustainability concerns in machining methods are critical.

In the presented study, as seen in Eq. (3), *CE* were calculated by summing the *CE* resulting from electricity consumption, material consumption, chip recycling, cutting fluid consumption, and cutting tool utilization. The indicators taken into account in the *CE* calculation and the *CE* equations of the relevant indicators taken from the study presented by Demir et al. [82] are shown in Fig. 8.

$$CE_{total} = CE_{el} + CE_{tool} + CE_{material} + CE_{chip} + CE_{c/l} \tag{3}$$

In calculating *CE* because of electricity consumption, the electricity consumption due to the idle (adjustment and return) movement of the tool, the electricity consumption due to the cutting process, and the electricity consumption of the MQL system used to transmit the cutting fluid to the cutting zone were collected (total energy consumption, E_{total}) and multiplied by Türkiye's electricity carbon emission factor (CEF_{el}). Türkiye's CEF_{el} value is 0.5434 $kgCO_2/kg$ [83]. Electricity consumption was calculated by multiplying the power spent for adjustment and return by their duration. The power consumed for adjustment and return is 0.4 kW [84]. The durations are 90 and 5 s, respectively. The electricity consumed for the cutting process was determined by multiplying the cutting power (P_c), obtained by multiplying F_c and V_c by the cutting time (t_c), which is the time spent on the cutting process. The electricity consumed by the MQL system was calculated by multiplying the power consumed by the MQL system, which is 0.425 kW [84], by the cutting time.

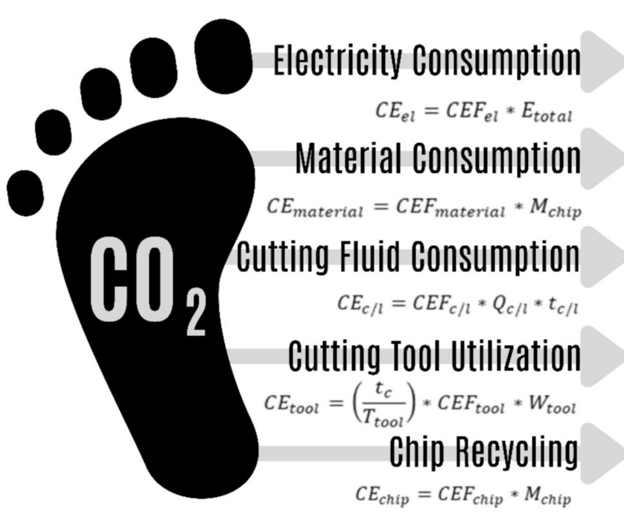

Fig. 8 Variables of total carbon emissions (the relevant equations were taken from Demir et al. [82])

In calculating *CE* due to material consumption and chip recycling, the chip weight (M_{chip}) is multiplied by the carbon emission factor of the material carbon emission factor ($CEF_{material}$) and the chip (CEF_{chip}), respectively. M_{chip} was calculated by multiplying the V_c, *f* value, a_p, t_c, and material density. $CEF_{material}$ and CEF_{chip} values are taken as 26.6 $kgCO_2/kg$ [85] and 0.87 $kgCO_2/kg$ [86], respectively.

The relation used to calculate *CE* resulting from the utilization of cutting tools (CE_{tool}) was given in Eq. (4). In this mathematical relationship, the ratio of t_c to tool life (T_{tool}) is multiplied by the cutting tool carbon emission factor (CEF_{tool}) and tool weight (W_{tool}) [82]. The W_{tool} used in the presented study is 15 g. The relation used to determine the CEF_{tool} is given in Eq. (5). The tool's energy consumption constant, denoted by the *K* value in the relation, is 1.5 MJ [87]. The equation based on V_c, f, a_p, hardness of workpiece (*H*), and MQL flow rate (*Q*) used to determine T_{tool} in the MQL method presented by El-Hossainy [88] is given in Eq. (6). The T_{tool} equation shown in Eq. (4) is provided for MQL conditions, and the MQL condition using vegetable-based cutting oil improves T_{tool} by 15.5% compared to dry conditions [82]. N-MQL condition using graphene-added vegetable-based cutting oil improves T_{tool} by 65.63% compared to dry-cutting [85].

$$CE_{tool} = \left(\frac{t_c}{T_{tool}}\right) * CEF_{tool} * W_{tool} \tag{4}$$

$$CEF_{tool} = \left(\frac{CEF_{el} * K}{3.6}\right) * \left(\frac{1000}{W_{tool}}\right) \tag{5}$$

$$T_{tool} = 2763 * V_c^{-0.3214} * f^{-0.2657} * a_p^{-0.2329} * H^{-1.12} * Q^{0.7529} \tag{6}$$

CE resulting from cutting fluid consumption ($CE_{c/l}$) was determined by multiplying the cutting fluid application time, MQL flow rate, and vegetable-based cutting fluid carbon emission factor ($CEF_{c/l}$). The cutting fluid flow rate was adjusted to 21 ml/h using the MQL system. The value of $CEF_{c/l}$ is 0.36 $kgCO_2/kg$ [89]. In order to determine the *CE* of nanofluids, the carbon emissions factors for nanoparticles were used to be 1520 $kgCO_2/kg$ [82].

Results for *CE* are displayed in Fig. 9. The *CE* decreased with the increase in *f* and V_c. Compared to the 30 m/min V_c, 35 m/min and 40 m/min V_c reduced *CE* by 2.1% and 3.7%, respectively. In addition, increasing the *f* value from 0.1 to 0.15 mm/rev reduced *CE* by 6.1%, while increasing it from 0.1 to 0.2 mm/rev reduced *CE* by 9.4%. Although *CE* resulting from tool wear increase with increasing *f* and V_c, decreasing machining time reduces *CE*. Also, it has been reported by Astakhov and Davim [90] that *f* is considered the most important resource in increasing productivity. As can be seen in Fig. 2, as the V_c increased, the T_c increased, and thermal softening occurred in the material. This resulted in a decrease in F_c, as seen in Fig. 4. Reducing F_c has reduced the P_c and *CE* resulting from electricity consumption.

The dry-cutting condition is considered a more sustainable process due to the absence of *CE* from the energy consumption of the MQL system and the use of cutting fluid [82]. However, in the presented study, dry cutting resulted in higher *CE* than other cutting conditions. Compared to dry-cutting conditions, MQL and N-MQL methods reduced *CE* by 2.6% and 10.5%, respectively. A similar result was also presented by Saatçi et al. [89]. There exist several factors contributing to this phenomenon. The T_{tool} is diminished in dry conditions, while the energy expended is augmented due to heightened F_c. Under MQL and N-MQL, *CE* due to the energy consumption of the MQL unit increase.

On the other hand, in these methods, energy consumption due to the cutting process decreases due to the decrease in F_c. In addition, as the T_{tool} is extended, the *CE* value from cutting tools decreases. While dry-cutting, 30 m/min V_c, and 0.1 mm/rev *f* value is the worst *CC* in terms of *CE*, N-MQL cutting condition, 40 m/min V_c, and 0.2 mm/rev *f* value is the best *CC* in terms of *CE*. As a result, *CE* were reduced by 21.55%.

Additionally, the *CE* were statistically analyzed. The contribution ratios of cutting parameters such as *CC*, V_c, and *f* to the *CE* were determined to be 47.45%, 5.69%, and 38.77%, respectively. The most effective interactions here are the CC^2 and $CC*f$, with contribution ratios of 4.14% and 1.97%, respectively.

3.2.2 Total Machining Costs (*MC*)

In calculating the total machining cost (*MC*), as seen in Fig. 10, costs resulting from the milling process $\left(MC_{milling}\right)$, energy consumption $\left(MC_{energy}\right)$, cutting fluid consumption $\left(MC_{fluid}\right)$, cutting tool $\left(MC_{tool}\right)$ and environmental impact $\left(MC_{environment}\right)$ were taken into account. The equation regarding the total machining cost is given in Eq. (7) [82].

$$MC = MC_{milling} + MC_{tool} + MC_{c/l} + MC_{energy} + MC_{environment} \tag{7}$$

In calculating the costs arising from the milling process ($MC_{milling}$), the total time spent by the cutting tool in the cutting process and idle was multiplied by the sum of labor and general expenses. The labor prices in the presented work are \$12/h, and the total overhead costs are \$35/h.

In calculating the cost resulting from the use of cutting tools (MC_{tool}), the ratio of t_c to T_{tool} was determined by multiplying it by the cutting tool cost. T_{tool} values for different cutting parameters and conditions were determined with the help of Eq. (6). The unit cost of the cutting tool is taken as \$3.55.

In calculating the costs resulting from cutting fluid consumption ($MC_{c/l}$), the unit cost of the cutting fluid was multiplied by the *Q* and t_c. Since there is no use of cutting fluid in dry conditions, the cost of cutting fluid consumption is zero. The unit costs of vegetable-based cutting fluid and nanographene powder are 8 \$/L and 1.5 \$/g, respectively. In

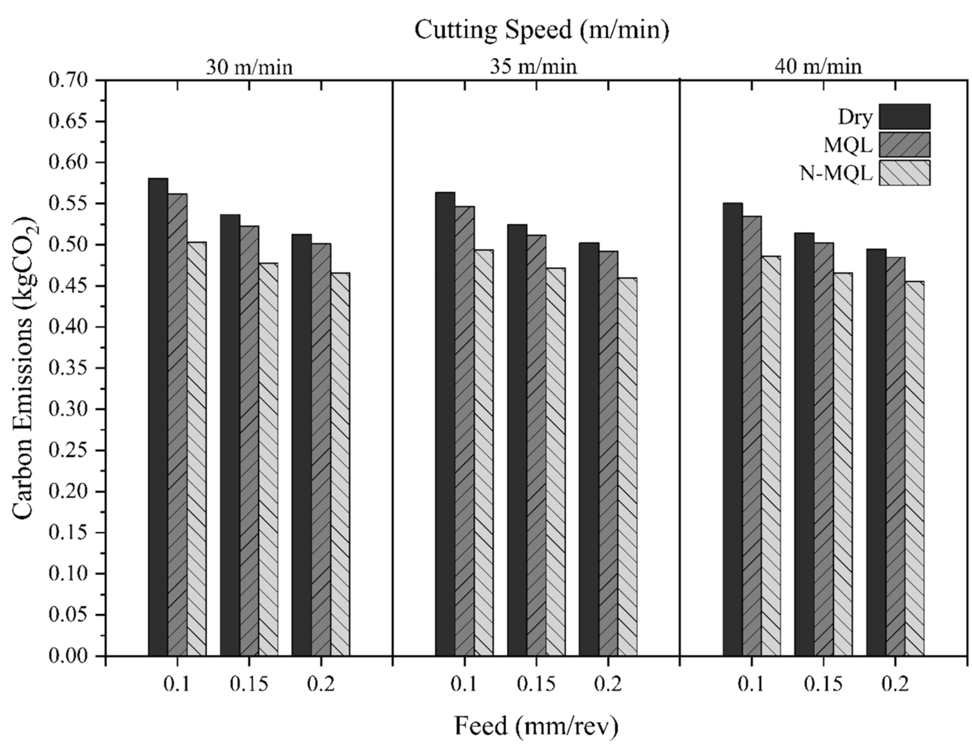

Fig. 9 The change in total carbon emissions under different cutting environments and parameters

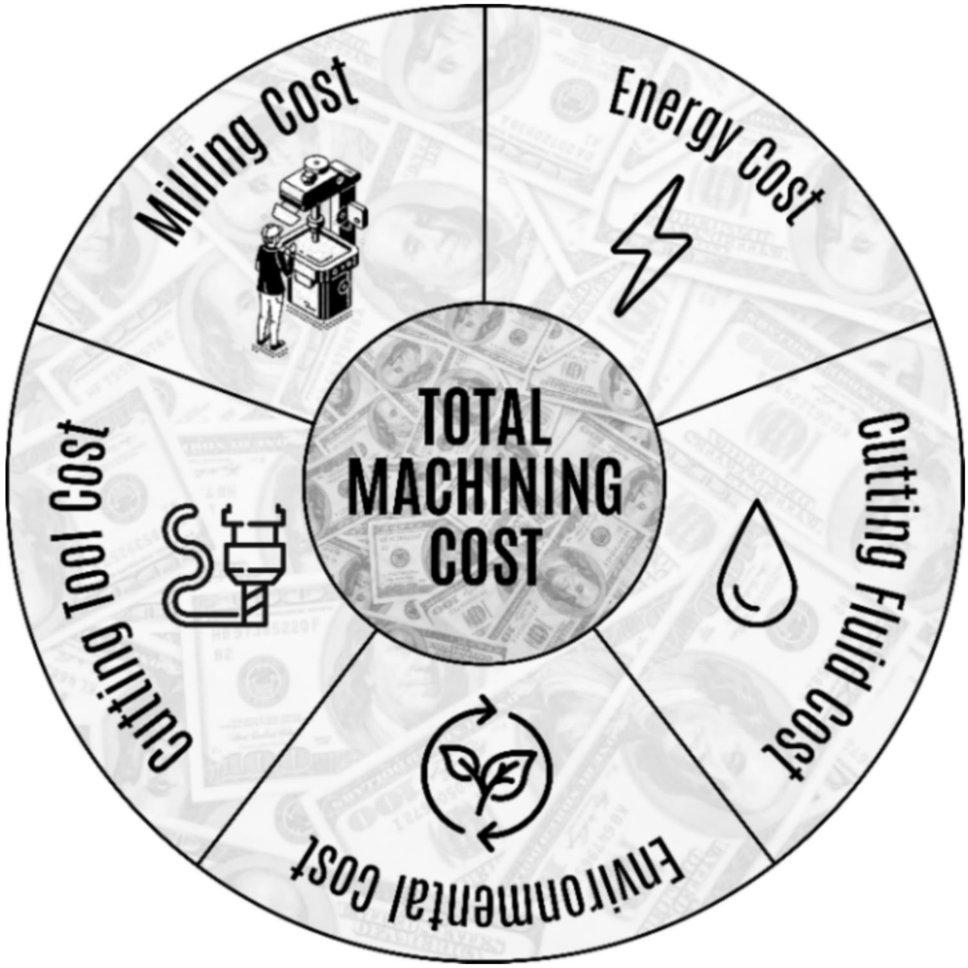

Fig. 10 Indicators taken into account in calculating total machining costs

the N-MQL, due to the addition of 0.8% by weight graphene to the vegetable-based cutting fluid, the unit cost of the fluid used according to the MQL method increases. The Q of 21 ml/h was employed for MQL and N-MQL conditions.

In calculating the costs arising from energy consumption (MC_{energy}), Türkiye's industry unit energy price was multiplied by the total consumed energy. Türkiye industrial unit energy price is taken as 0.067 $/kWh.

A cost arises due to the impact of *CE* on the environment ($MC_{environment}$). The ecological load cost and *CE* were multiplied to calculate the environmental cost. The ecological load cost is taken from the study presented by Uysal and Jawahir [91], and its value is 0.025 $/kg.

The results of the *MC* are given in Fig. 11. Increasing the V_c from 30 to 35 m/min reduced the *MC* by 7.0% while increasing it from 30 to 40 m/min reduced the *MC* by 12.4%. As the V_c was augmented, there was a corresponding rise in the temperature of the cutting process. The observed phenomenon led to thermal softening of the material, hence reducing F_c. The reduction in F_c led to decreased P_c and resulted in lower *MC* associated with energy consumption. The *MC* was lowered by 18.5% when the *f* value was increased from 0.1 to 0.15 mm/rev and by 28.4% when it was increased from 0.1 to 0.2 mm/rev. As *f* value increases, the expenses associated with tool utilization tend to rise, but the costs attributed to energy consumption tend to decline due to reduced t_c.

If the *CC* are examined, the MQL and N-MQL methods reduced *MC* by 6.8% and 25.6%, respectively, compared to dry-cutting environment. While the dry-cutting, 30 m/min V_c, and 0.1 mm/rev *f* value is the worst *CC* in terms of *MC*, N-MQL condition, 40 m/min V_c, and 0.2 mm/rev *f* value is the best *CC* in terms of *MC*. As a result, *MC* were reduced by 52.6%.

Additionally, the *MC* were statistically analyzed. The contribution ratios of cutting parameters such as *CC*, V_c, and *f* to the *MC* were determined to be 36.13%, 7.63%, and 49.64%, respectively. The most effective interactions here

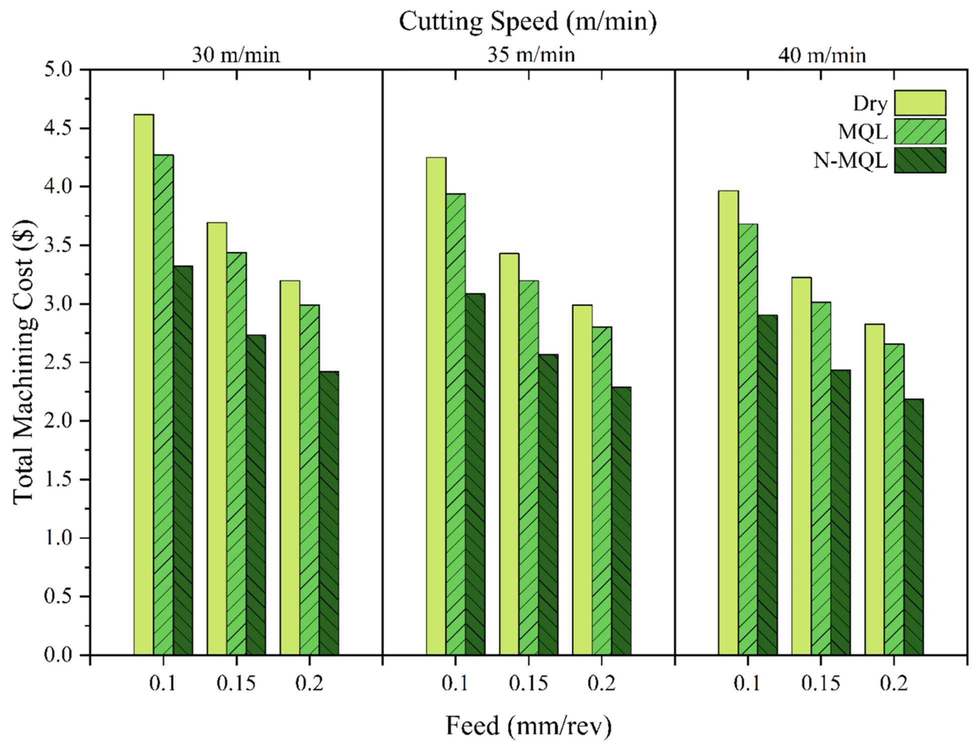

Fig. 11 The change in total machining costs under different cutting environments and parameters

are the s CC^2 and $CC*f$, with contribution ratios of 2.63% and 1.56%, respectively.

3.3 Multi-objective Optimization and Multi-criteria Decision-Making

The F_c, T_c, R_a, *CE*, and *MC* results obtained as a result of this study are desired to be low. However, as can be seen from the results, the parameters of an experiment decrease some results and increase some results. Therefore, it is necessary to use multi-objective optimization (MOOP) and multi-criteria decision-making (MCDM) to select appropriate cutting conditions and parameters. In this study, *CE* and *MC*-weighted optimization was performed using a combination of NSGA-II (non-dominant sequencing genetic algorithm II) and VIKOR methods. Although VIKOR has been used to determine optimum cutting parameters in machining problems [92], there are a limited number of studies in which it is used as a hybrid with NSGA-II [93]. Additionally, there is uncertainty in using this hybrid optimization method in sustainability assessment. A flow chart of the process for maximizing sustainability through the utilization of NSGA-II and VIKOR is given in Fig. 12.

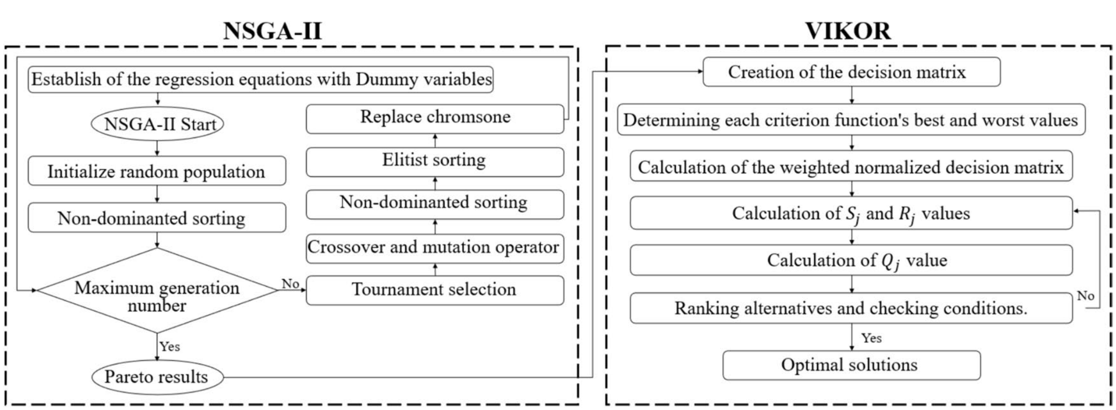

Fig. 12 NSGA-II and VIKOR-based sustainability optimization flow chart

Table 6 Dummy variables for cutting conditions

Cutting conditions (*CC*)	CC_1	CC_2
Dry	1	0
MQL	0	1
N-MQL	0	0

First, dummy variables were used to code the *CC*, which were in text format, by converting them into number format. Dummy variables are categorical variables that can only have two values, typically represented as 1 or 0 [89]. In this context, the value of 1 indicates the existence of a qualitative characteristic that has an impact on the outcome, while a value of 0 indicates the lack of this characteristic, which has no influence on the result. *CC* are coded numerically with the help of dummy variables, as seen in Table 6.

After creating dummy variables, regression equations were established using the experimental and sustainability analysis results, which are cutting force, cutting temperature, surface roughness, carbon emission and machining cost. The established regression equations are given in Eqs. (8–12) and their adequacy is measured from the R^2 value. The R^2 values for F_c, T_c, R_a, *CE*, and *MC* are 98.32%, 97.6%, 97.83%, 99.93% and 99.93%, respectively.

$$F_c = 75 + 84.2 * CC_1 + 14.2 * CC_2 + 1.8 * V_c + 2165 * f - 0.07 * V_c^2 - 2215 * f^2 - 0.18 * CC_1 * V_c - 68 * CC_1 * f - 1.13 * CC_2 * V_c + 270 * CC_2 * f + 4.5 * V_c * f \tag{8}$$

$$T_c = 49.6 - 5.38 * CC_1 - 2.52 * CC_2 - 1.22 * V_c - 43 * f + 0.0169 * V_c^2 + 76 * f^2 + 0.479 * CC_1 * V_c + 23.1 * CC_1 * f + 0.153 * CC_2 * V_c + 12.3 * CC_2 * f + 2.57 * V_c * f \tag{9}$$

$$R_a = -2.46 + 0.295 * CC_1 + 1.146 * CC_2 + 0.186 * V_c - 16.9 * f - 0.00215 * V_c^2 + 74.2 * f^2 + 0.0135 * CC_1 * V_c - 0.34 * CC_1 * f + 0.036 * CC_2 * V_c + 3.14 * CC_2 * f + 0.308 * V_c * f \tag{10}$$

$$CE = 0.7383 + 0.13417 * CC_1 + 0.10221 * CC_2 - 0.00577 * V_c - 1.5907 * f + 0.000043 * V_c^2 + 3.005 * f^2 - 0.001056 * CC_1 * V_c - 0.2772 * CC_1 * f - 0.000815 * CC_2 * V_c - 0.211 * CC_2 * f + 0.00998 * V_c * f \tag{11}$$

$$MC = 8.883 + 2.243 * CC_1 + 1.646 * CC_2 - 0.1425 * V_c - 35.94 * f + 0.00107 * V_c^2 + 65.17 * f^2 - 0.01787 * CC_1 * V_c - 4.673 * CC_1 * f - 0.01311 * CC_2 * V_c - 3.429 * CC_2 * f + 0.2385 * V_c * f \tag{12}$$

After establishing the regression equations, the equations were optimized with the NSGA-II method. The MOOP problem with the goals of reducing F_c, T_c, R_a, *CE*, and *MC* values was coded using MATLAB software. Similarly, a genetic algorithm was used by Sim and Lee [94] to obtain the optimum processing conditions that would minimize the production cost and machining time. The process steps in applying the NSGA-II method are listed in Fig. 12. The population size of the NSGA-II method was set to 30 and 30 outputs were requested. Furthermore, a limit of 20,000 generations was selected as the maximum number. The input parameters, which are cutting conditions (CC_1 and CC_2), V_c, and f, were defined based on the minimum and maximum values of the parameters.As a result of all these, a total of 30 Pareto optimal solutions were obtained. Contour plots of Pareto optimal solutions are given in Fig. 13.

VIKOR, one of the MCDM methods, was used to sort and select the Pareto optimum solutions determined by NSGA-II. The process steps applied in ranking the NSGA-II optimized results based on *CE* and *MC* using the VIKOR method are given below:

Step 1: Creating the decision matrix from the Pareto optimal results obtained as a result of NSGA-II.

Step 2: Determining each criterion function's best f_i^* and worst f_i^- values, $i = 1, 2, 3, \ldots, n$. The best and worst values for each evaluation criterion are determined according to the cost/benefit orientation of the criterion. In the presented study, the values of F_c, T_c, R_a, *CE*, and *MC* criteria are required to be low. Therefore, if the ith function is cost-oriented:

$$f_i^* = \min_j f_{ij} \ and \ f_i^- = \max_j f_{ij} \tag{13}$$

Step 3: Normalization process and creation of normalized matrix. Linear normalization method was used for normalization and each value was normalized and a normalized matrix was created. Since the criteria should be minimum in the best case, the equation given below was used.

$$\left(f_i^* - f_{ij}\right) / \left(f_i^* - f_i^-\right) \tag{14}$$

Step 4: Weighting of normalized decision matrix. The weighted normalized decision matrix is created by multiplying the normalized decision matrix with the importance levels of each criterion. Since an optimization based on *CE* and *MC* was made in the presented study, weights of 0.1, 0.1, 0.1, 0.35 and 0.35 were used for F_c, T_c, R_a, *CE*, and *MC*, respectively.

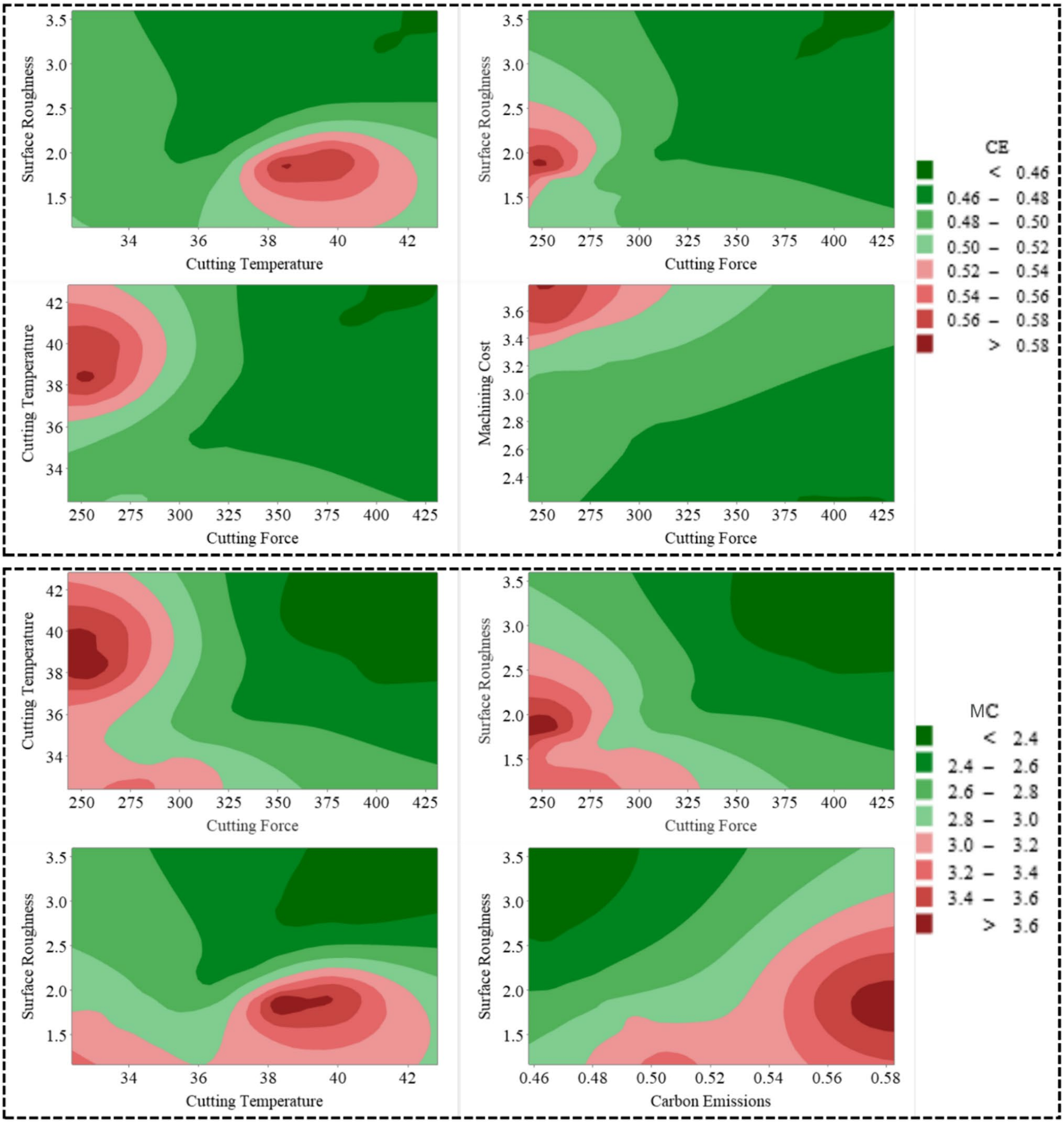

Fig. 13 Contour plots of Pareto optimal solutions

$$w_i * \left(f_i^* - f_{ij}\right) / \left(f_i^* - f_i^-\right) \tag{15}$$

Step 5: Calculation of S_j and R_j values, $j = 1, 2, 3, \ldots, J$.

$$S_j = \sum_{i=1}^{n} w_i * \left(\left(f_i^* - f_{ij}\right) / \left(f_i^* - f_i^-\right)\right) \tag{16}$$

$$R_j = \max_i \left[w_i * \left(\left(f_i^* - f_{ij}\right) / \left(f_i^* - f_i^-\right)\right)\right] \tag{17}$$

Step 6: Calculation of Q_j value. In order to calculate the Q_j value, S^*, S^-, R^*, and R^- values were determined based on the calculated S_j and R_j values. The variable v represents the weight assigned to the approach of maximizing the group utility by considering the majority of criteria. In this case, v is set to 0.5.

$$Q_j = v * \frac{(S_j - S^*)}{(S^- - S^*)} + (1 - v) * \frac{(R_j - R^*)}{(R^- - R^*)} \quad (18)$$

$$S^* = \min_j S_j \text{ and } S^- = \max_j S_j \quad (19)$$

$$R^* = \min_j R_j \text{ and } R^- = \max_j R_j \quad (20)$$

Step 7: Ranking alternatives and checking conditions. Alternatives were ranked from smallest to largest according to their calculated Q_j values. The decision of whether the alternative ranked first in the resulting ranking is the best was evaluated according to the conditions stated below.

Condition 1) This condition is called acceptable advantage. There is a condition that $Q(a^u) - Q(a^t) \geq DQ$ equality must be met. Here, a^t is a compromise option, which is considered the most favorable according to the Q (minimum) and a^u is the second-ranked alternative in the ranking list. DQ is defined by the equation $DQ = 1/(J - 1)$ and the number of alternatives (J) is taken as five (due to cutting force, cutting temperature, surface roughness, carbon emissions and machining cost).

Condition 2) The criterion for "acceptable stability in decision-making" is that alternative a^t must be regarded as the best by either S or R, or both.

These two conditions must be met, and the $v = 0.5$ value used in the presented study satisfied both conditions. The results ranked and selected by VIKOR are given in Table 6. The sorting is performed with the aim of a more sustainable machining, with emphasis *CE* and *MC*. As can be seen from the table, the most sustainable *CC* is N-MQL method. As is known, in the presented study, 30, 35, and 40 m/min were used for V_c, and 0.1, 0.15, and 0.2 were used for f value. As can be seen in Table 7, from the sustainability-based optimization results, it was determined that the approximate V_c should be selected between 36 and 40 m/min and the f should be selected between 0.14 and 0.18 mm/rev. Using the N-MQL method at above-average V_c and f values is the most sustainable machining parameters and *CC* for milling of Al6082.

4 Conclusion

In the presented study, MQL method using graphane added-nanofluid (N-MQL) was used for the first time in the milling of Al6082 alloy, and its machining responses (cutting temperature, cutting force, feed force, surface roughness, and chip morphology) and sustainability indicators (carbon emission and total machining cost) were determined and compared with dry and vegetable-based cutting oil MQL methods. Then, applying multi-objective optimization using NSGA-II (non-dominant sequencing genetic algorithm II) and the multi-criteria decision-making method using VIKOR, optimum process parameters were determined in terms of sustainability-weighed carbon emissions and total machining cost. The conclusions collected after analyzing the information gathered during the current study are as follows:

- The utilization of the N-MQL cutting condition, as opposed to the dry cutting condition with appropriate cutting parameters, resulted in improvements of 50.6% in cutting force, 65.4% in feed force, 50.6% in cutting temperature, 67.3% in surface roughness, 33.2% in chip width, 15.3% in chip length, 21.5% in carbon emissions, and 52.6% in machining cost.
- The MQL method using graphene nanofluid holds great promise for improving the efficiency and sustainability of aluminum alloy machining.
- From the sustainability-based optimization results, which is carbon emissions and total machining cost-weighted optimization, it was determined that the cutting speed should be selected between 36 and 40 m/min, the feed should be selected between 0.14 and 0.18 mm/rev, and the N-MQL method should be used.
- Cutting condition was determined as the most effective parameter in both carbon emission and machining cost, with contribution ratios of 47.45% and 36.13%, respectively. The cutting condition is followed by feed with contribution rates of 38.77% and 49.64%.
- NSGA-II and VIKOR-based sustainability assessment and optimization enabled the aluminum machining process to be evaluated from environmental, economic and machinability perspectives.

Table 7 Optimal selected and ranked results by VIKOR

Rank	*CC*	V_c (m/min)	f (mm/rev)	F_c (N)	T_c (°C)	R_a (µm)	*CE* (kgCO_2)	*MC* ($)
1	N-MQL	36.41	0.155	355.5	37.2	2.363	0.46718	2.45409
2	N-MQL	36.18	0.146	341.6	36.5	2.200	0.47027	2.52758
3	N-MQL	40.00	0.172	373.2	40.4	2.953	0.46022	2.28112
4	N-MQL	36.09	0.141	332.6	36.1	2.109	0.47238	2.57725
5	N-MQL	40.00	0.178	382.5	40.9	3.079	0.45940	2.26014

In future studies, it is possible to attain a more efficient and proficient evaluation and improvement of sustainability in relation to carbon emissions and total machining costs by employing alternative machine learning and deep learning algorithms instead of NSGA-II.

Declarations

Conflict of interest The authors declare that they have no known competing financial interests or personal relationships that could have appeared to influence the work reported in this paper.

References

1. Arunakumara, P. C., Sagar, H. N., Gautam, B., George, R., & Rajeesh, S. (2023). A review study on fatigue behavior of aluminum 6061 T-6 and 6082 T-6 alloys welded by MIG and FS welding methods. *Materials Today: Proceedings, 74*(2), 293–301. https://doi.org/10.1016/j.matpr.2022.08.242
2. Karupannasamy, D. K., Sasikumar, K. S. K., & Shankar, S. (2020). Experimental and numerical analysis of impact strength of Al6082 for automotive structural applications. *Materials Today: Proceedings, 33*(7), 2863–2867. https://doi.org/10.1016/j.matpr.2020.02.747
3. Hosseinabadi, O. F., & Khedmati, M. R. (2021). A review on ultimate strength of aluminium structural elements and systems for marine applications. *Ocean Engineering, 232*, 109153. https://doi.org/10.1016/j.oceaneng.2021.109153
4. Yin, L., Ni, Z., Li, J., Fan, F., Zhi, X., Ye, J., Pan, Y., & Guo, Y. (2023). High-temperature mechanical properties of constructional 6082-T6 aluminum alloy extrusion. *Structures, 48*, 1244–1258. https://doi.org/10.1016/j.istruc.2023.01.043
5. Wu, J., Zhang, C., Lian, K., Cao, H., & Li, C. (2022). Carbon emission modeling and mechanical properties of laser, arc and laser–arc hybrid welded aluminum alloy joints. *Journal of Cleaner Production, 378*, 134437. https://doi.org/10.1016/j.jclepro.2022.134437
6. Soo, V. K., Peeters, J., Paraskevas, D., Compston, P., Doolan, M., & Duflou, J. R. (2018). Sustainable aluminium recycling of end-of-life products: A joining techniques perspective. *Journal of Cleaner Production, 178*, 119–132. https://doi.org/10.1016/j.jclepro.2017.12.235
7. Yücel, A., Yıldırım, Ç. V., Sarıkaya, M., Şirin, Ş, Kıvak, T., Gupta, M. K., & Tomaz, Í. V. (2021). Influence of MoS2 based nanofluid-MQL on tribological and machining characteristics in turning of AA 2024 T3 aluminum alloy. *Journal of Materials Research and Technology, 15*, 1688–1704. https://doi.org/10.1016/j.jmrt.2021.09.007
8. Sarikaya, M., Gupta, M. K., Tomaz, I., Danish, M., Mia, M., Rubaiee, S., Jamil, M., Pimenov, D. Y., & Khanna, N. (2021). Cooling techniques to improve the machinability and sustainability of light-weight alloys: A state-of-the-art review. *Journal of Manufacturing Processes, 62*, 179–201. https://doi.org/10.1016/j.jmapro.2020.12.013
9. Davim, J. P. (2013). *Sustainable manufacturing* (pp. 79–110). Wiley.
10. Davim, J. P. (2024). Sustainable and intelligent manufacturing: Perceptions in line with 2030 agenda of sustainable development. *BioResources, 19*(1), 4–5.
11. Davim, J. P. (2008). *Machining: fundamentals and recent advances*. Springer.
12. Xu, J., Ji, M., Davim, J. P., Chen, M., El Mansori, M., & Krishnaraj, V. (2020). Comparative study of minimum quantity lubrication and dry drilling of CFRP/titanium stacks using TiAlN and diamond coated drills. *Composite Structures, 234*, 111727. https://doi.org/10.1016/j.compstruct.2019.111727
13. Krolczyk, G. M., Maruda, R. W., Krolczyk, J. B., Wojciechowski, S., Mia, M., Nieslony, P., & Budzik, G. (2019). Ecological trends in machining as a key factor in sustainable production—A review. *Journal of Cleaner Production, 218*, 601–615. https://doi.org/10.1016/j.jclepro.2019.02.017
14. Carou, D., Rubio, E. M., & Davim, J. P. (2015). A note on the use of the minimum quantity lubrication (MQL) system in turning. *Industrial Lubrication and Tribology, 67*(3), 256–261. https://doi.org/10.1108/ILT-07-2014-0070
15. Maruda, R. W., Szczotkarz, N., Wojciechowski, S., Gawlik, J., & Królczyk, G. M. (2023). Metrological relations between the spray atomization parameters of a cutting fluid and formation of a surface topography and cutting force. *Measurement, 219*, 113255. https://doi.org/10.1016/j.measurement.2023.113255
16. Davim, J. P., Sreejith, P. S., Gomes, R., & Peixoto, C. (2006). Experimental studies on drilling of aluminium (AA1050) under dry, minimum quantity of lubricant, and flood-lubricated conditions. *Proceedings of the Institution of Mechanical Engineers, Part B: Journal of Engineering Manufacture, 220*(10), 1605–1611. https://doi.org/10.1243/09544054JEM557
17. Nandi, A. K., & Davim, J. P. (2009). A study of drilling performances with minimum quantity of lubricant using fuzzy logic rules. *Mechatronics, 19*(2), 218–232. https://doi.org/10.1016/j.mechatronics.2008.08.004
18. Kishawy, H. A., Dumitrescu, M., Ng, E. G., & Elbestawi, M. A. (2005). Effect of coolant strategy on tool performance, chip morphology and surface quality during high-speed machining of A356 aluminum alloy. *International Journal of Machine Tools and Manufacture, 45*(2), 219–227. https://doi.org/10.1016/j.ijmachtools.2004.07.003
19. Tosun, N., & Huseyinoglu, M. (2010). Effect of MQL on surface roughness in milling of AA7075-T6. *Materials and Manufacturing Processes, 25*(8), 793–798. https://doi.org/10.1080/10426910903496821
20. Joshua, O. S., David, M. O., & Sikiru, I. O. (2015). Experimental investigation of cutting parameters on surface roughness prediction during end milling of aluminium 6061 under MQL (minimum quantity lubrication). *Journal of Mechanical Engineering and Automation, 5*(1), 1–13. https://doi.org/10.5923/j.jmea.20150501.01
21. Khettabi, R., Nouioua, M., Djebara, A., & Songmene, V. (2017). Effect of MQL and dry processes on the particle emission and part quality during milling of aluminum alloys. *International Journal of Advanced Manufacturing Technology, 92*, 2593–2598. https://doi.org/10.1007/s00170-017-0339-5
22. Conger, D. B., Emiroğlu, U., Uysal, A., & Altan, E. (2019). An experimental study on cutting forces and surface roughness in MQL Milling of Al6061. *Machines. Technologies. Materials, 13*(2), 86–89.
23. Zhu, G., Yuan, S., & Chen, B. (2019). Numerical and experimental optimizations of nozzle distance in minimum quantity lubrication (MQL) milling process. *International Journal of Advanced Manufacturing Technology, 101*, 565–578. https://doi.org/10.1007/s00170-018-2928-3
24. Imthiyas, A., Kumar, S. K., Krishna, B. A., Robinson, G., & Suriya, S. (2023). Experimental investigation on surface roughness of aluminum alloy 6063 machining with minimum quantity lubricant. *AIP Conference Proceedings, 2523*, 020128. https://doi.org/10.1063/5.0112460

25. Gupta, M. K., Jamil, M., Wang, X., Song, Q., Liu, Z., Mia, M., Hegab, H., Khan, A. M., Collado, A. G., Pruncu, C. I., & Shah Imran, G. M. (2019). Performance evaluation of vegetable oil-based nano-cutting fluids in environmentally friendly machining of Inconel-800 Alloy. *Materials, 12*(17), 2792. https://doi.org/10.3390/ma12172792
26. Sharma, A. K., Tiwari, A. K., & Dixit, A. R. (2017). Effects of minimum quantity lubrication (MQL) in machining processes using conventional and nanofluid based cutting fluids: A comprehensive review. *Journal of Cleaner Production, 141*, 1008–1030. https://doi.org/10.1016/j.jclepro.2016.09.130
27. Maruda, R. W., Arkusz, K., Szczotkarz, N., Wojciechowski, S., Niesłony, P., & Królczyk, G. M. (2023). Analysis of size and concentration of nanoparticles contained in cutting fluid during turning of 316L steel in minimum quantity lubrication conditions. *Journal of Manufacturing Processes, 87*, 106–122. https://doi.org/10.1016/j.jmapro.2022.12.065
28. Maruda, R. W., Szczotkarz, N., Michalski, M., Arkusz, K., Wojciechowski, S., Niesłony, P., Khanna, N., & Królczyk, G. M. (2023). Evaluation of tool wear during turning of Ti6Al4V alloy applying MQL technique with Cu nanoparticles diversified in terms of size. *Wear, 532–533*, 205111. https://doi.org/10.1016/j.wear.2023.205111
29. Rahmati, B., Sarhan, A. A. D., & Sayuti, M. (2014). Morphology of surface generated by end milling AL6061-T6 using molybdenum disulfide (MoS2) nanolubrication in end milling machining. *Journal of Cleaner Production, 66*, 685–691. https://doi.org/10.1016/j.jclepro.2013.10.048
30. Najiha, M. S., & Rahman, M. M. (2016). Experimental investigation of flank wear in end milling of aluminum alloy with water-based TiO_2 nanofluid lubricant in minimum quantity lubrication technique. *International Journal of Advanced Manufacturing Technology, 86*, 2527–2537. https://doi.org/10.1007/s00170-015-8256-y
31. Yuan, S., Hou, X., Wang, L., & Chen, B. (2018). Experimental investigation on the compatibility of nanoparticles with vegetable oils for nanofluid minimum quantity lubrication machining. *Tribology Letters, 66*, 106. https://doi.org/10.1007/s11249-018-1059-1
32. Kulkarni, H. B., Nadakatti, M. M., Kulkarni, S. C., & Kulkarni, R. M. (2020). Investigations on effect of nanofluid based minimum quantity lubrication technique for surface milling of Al7075-T6 aerospace alloy. *Materials Today: Proceedings, 27*(1), 251–256. https://doi.org/10.1016/j.matpr.2019.10.127
33. Raza, M. H., Hafeez, F., Zhong, R. Y., & Imran, A. (2020). Investigation of surface roughness in face milling processes. *International Journal of Advanced Manufacturing Technology, 111*, 2589–2599. https://doi.org/10.1007/s00170-020-06188-8
34. Gao, W., Qi, Q., Dong, L., Lv, X., & Huang, W. (2021). Experimental evaluation of the lubrication performance of milling Al7075 with different nanofluids MQL. *Journal of Physics: Conference Series, 1744*, 022142. https://doi.org/10.1088/1742-6596/1744/2/022142
35. Safiei, W., Rahman, M. M., Yusoff, A. R., et al. (2021). Effects of SiO_2–Al_2O_3–ZrO_2 tri-hybrid nanofluids on surface roughness and cutting temperature in end milling process of aluminum alloy 6061-T6 using uncoated and coated cutting inserts with minimal quantity lubricant method. *Arabian Journal for Science and Engineering, 46*, 7699–7718. https://doi.org/10.1007/s13369-021-05533-7
36. Bhavsar, H., & Kulkarni, S. R. (2022). Taguchi design optimization of the AA6063 CNC end milling process with minimum quantity lubrication and SiO_2 based nanofluid. *International Journal for Research in Applied Science and Engineering Technology, 10*(9), 1466–1472. https://doi.org/10.2221/ijraset.2022.46862
37. Tiwari, R. S., Vats, P., Singh, T., Dubey, V., Arora, P. K., & Sharma, A. K. (2023). An ınvestigation on effect of hybrid nanofluids in end milling of aluminium 6061 alloy. In S. Yadav, P. K. Jain, P. K. Kankar, & Y. Shrivastava (Eds.), *Lecture notes in mechanical engineering*. Singapore: Springer. https://doi.org/10.1007/978-981-19-1618-2_9
38. Alqahtani, B., Hoziefa, W., Abdel Moneam, H. M., Hamoud, M., Salunkhe, S., Elshalakany, A. B., Abdel-Mottaleb, M., & Davim, J. P. (2022). Tribological performance and rheological properties of engine oil with graphene nano-additives. *Lubricants, 10*, 137. https://doi.org/10.3390/lubricants10070137
39. Ismail, N. A., Zulkifli, N. W. M., Chowdhury, Z. Z., & Johan, M. R. (2021). Functionalization of graphene-based materials: Effective approach for enhancement of tribological performance as lubricant additives. *Diamond and Related Materials, 115*, 108357. https://doi.org/10.1016/j.diamond.2021.108357
40. Gao, Q., Liu, S., Hou, K., Li, Z., & Wang, J. (2022). Graphene-based nanomaterials as lubricant additives: A review. *Lubricants, 10*, 273. https://doi.org/10.3390/lubricants10100273
41. Park, K., Ewald, B., & Kwon, P. Y. (2011). Effect of nano-enhanced lubricant in minimum quantity lubrication balling milling. *Journal of Tribology, 133*(3), 031803. https://doi.org/10.1115/1.4004339
42. Uysal, A. (2016). Investigation of flank wear in MQL milling of ferritic stainless steel by using nano graphene reinforced vegetable cutting fluid. *Industrial Lubrication and Tribology, 68*(4), 446–451. https://doi.org/10.1108/ILT-10-2015-0141
43. Pavan, R. B., Gopal, A. V., Amrita, M., & Goriparthi, B. K. (2019). Experimental investigation of graphene nanoplatelets-based minimum quantity lubrication in grinding Inconel 718. *Proceedings of the Institution of Mechanical Engineers, Part B: Journal of Engineering Manufacture, 233*(2), 400–410. https://doi.org/10.1177/0954405417728311
44. Uysal, A. (2017). An experimental study on cutting temperature and burr in milling of ferritic stainless steel under MQL using nano graphene reinforced cutting fluid. *Advanced Materials Proceedings, 2*(9), 560–563. https://doi.org/10.5185/amp.2017/038
45. Huang, W. T., Yang, W. K., Chiang, T. L., & Chou, J. H. (2018). The application of nanofluid (nanographene)/ultrasonic atomization micro-lubrication in micro-milling process on SKD11 die steel. In *International Conference on System Science and Engineering (ICSSE), New Taipei, Taiwan*. https://doi.org/10.1109/ICSSE.2018.8520247
46. Pal, A., Chatha, S. S., & Sidhu, H. S. (2020). Experimental investigation on the performance of MQL drilling of AISI 321 stainless steel using nanographene enhanced vegetable-oil-based cutting fluid. *Tribology International, 151*, 106508. https://doi.org/10.1016/j.triboint.2020.106508
47. Sahoo, S. P., & Datta, S. (2020). Dry, MQL, and nanofluid MQL machining of Ti–6Al–4V using uncoated WC-Co insert: Application of Jatropha oil as base cutting fluid and graphene nanoplatelets as additives. *Arabian Journal for Science and Engineering, 45*, 9599–9618. https://doi.org/10.1007/s13369-020-04849-0
48. Baldin, V., Ribeiro da Silva, L. R., Houck, C. F., Gelamo, R. V., & Machado, Á. R. (2021). Effect of graphene addition in cutting fluids applied by MQL in end milling of AISI 1045 steel. *Lubricants, 9*, 70. https://doi.org/10.3390/lubricants9070070
49. Danish, M., Gupta, M. K., Rubaiee, S., Ahmed, A., & Sarikaya, M. (2021). Influence of graphene reinforced sunflower oil on thermo-physical, tribological and machining characteristics of inconel 718. *Journal of Materials Research and Technology, 15*, 135–150. https://doi.org/10.1016/j.jmrt.2021.07.161
50. Min, Y., Hwang, Y. H., & Kim, D. E. (2024). Tribological properties of CNT microspheres as a lubricant additive. *International*

Journal of Precision Engineering and Manufacturing, 25, 639–646. https://doi.org/10.1007/s12541-024-00956-2

51. Touggui, Y., Uysal, A., Emiroglu, U., Belhadi, S., & Temmar, M. (2021). Evaluation of MQL performances using various nanofluids in turning of AISI 304 stainless steel. *International Journal of Advanced Manufacturing Technology, 115*, 3983–3997. https://doi.org/10.1007/s00170-021-07448-x
52. Klazly, M., & Bognár, G. (2022). A novel empirical equation for the effective viscosity of nanofluids based on theoretical and empirical results. *International Communications in Heat and Mass Transfer, 135*, 106054. https://doi.org/10.1016/j.icheatmasstransfer.2022.106054
53. Yıldırım, Ç. V., Şirin, Ş., Kıvak, T., & Sarıkaya, M. (2022). A comparative study on the tribological behavior of mono&proportional hybrid nanofluids for sustainable turning of AISI 420 hardened steel with cermet tools. *Journal of Manufacturing Processes, 73*, 695–714. https://doi.org/10.1016/j.jmapro.2021.11.044
54. Corcione, M. (2011). Empirical correlating equations for predicting the effective thermal conductivity and dynamic viscosity of nanofluids. *Energy Conversion and Management, 52*, 789–793. https://doi.org/10.1016/j.enconman.2010.06.072
55. Şirin, E., Kıvak, T., & Yıldırım, Ç. V. (2021). Effects of mono/hybrid nanofluid strategies and surfactants on machining performance in the drilling of Hastelloy X. *Tribology International, 157*, 106894. https://doi.org/10.1016/j.triboint.2021.106894
56. Uysal, A., & Jawahir, I. S. (2021). Analysis of slip-line model for serrated chip formation in orthogonal machining of AISI 304 stainless steel under various cooling/lubricating conditions. *Journal of Manufacturing Processes, 67*, 447–460. https://doi.org/10.1016/j.jmapro.2021.05.009
57. Kumar, A., Sharma, A. K., & Katiyar, J. K. (2023). State-of-the-art in sustainable machining of different materials using nano minimum quality lubrication (NMQL). *Lubricants, 11*, 64. https://doi.org/10.3390/lubricants11020064
58. Santos, M. C., Machado, A. R., & Barrozo, M. A. S. (2018). Temperature in machining of aluminum alloys. *Temparature Sensing*. https://doi.org/10.5772/intechopen.75943
59. Leonidas, E., Ayvar-Soberanis, S., Laalej, H., Fitzpatrick, S., & Willmott, J. R. (2022). A comparative review of thermocouple and infrared radiation temperature measurement methods during the machining of metals. *Sensors, 22*, 4693. https://doi.org/10.3390/s2213469
60. Abukhshim, N. A., Mativenga, P. T., & Sheikh, M. A. (2006). Heat generation and temperature prediction in metal cutting: A review and implications for high speed machining. *International Journal of Machine Tools and Manufacture, 46*, 782–800. https://doi.org/10.1016/j.ijmachtools.2005.07.024
61. Alojali, H. M., & Benyounis, K. Y. (2016). Advances in tool wear in turning process. In: *Reference module in materials science and materials engineering*. Elsevier. https://doi.org/10.1016/B978-0-12-803581-8.04031-5
62. Kong, L., Sun, J., & Bao, Y. (2017). Preparation, characterization and tribological mechanism of nanofluids. *RSC Advances, 7*, 12599–12609. https://doi.org/10.1039/C6RA28243A
63. Alves, S., Barros, B., Trajano, M., Ribeiro, K., & Moura, E. (2013). Tribological behavior of vegetable oil-based lubricants with nanoparticles of oxides in boundary lubrication conditions. *Tribology International, 65*, 28–36. https://doi.org/10.1016/j.triboint.2013.03.027
64. Pal, A., Chatha, S. S., & Sidhu, H. S. (2022). Assessing the lubrication performance of various vegetable oil-based nano-cutting fluids via eco-friendly MQL technique in drilling of AISI 321 stainless steel. *Journal of the Brazilian Society of Mechanical Sciences and Engineering, 44*, 148. https://doi.org/10.1007/s40430-022-03442-w
65. Zulkifli, N., Kalam, M., Masjuki, H., & Yunus, R. (2013). Experimental analysis of tribological properties of biolubricant with nanoparticle additive. *Procedia Engineering, 68*, 152–157. https://doi.org/10.1016/j.proeng.2013.12.161
66. Yusaf, T., Mahamude, A. S. F., Farhana, K., Harun, W. S. W., Kadirgama, K., Ramasamy, D., Kamarulzaman, M. K., Subramonian, S., Hall, S., & Dhahad, H. A. (2022). A comprehensive review on graphene nanoparticles: Preparation, properties, and applications. *Sustainability, 14*, 12336. https://doi.org/10.3390/su141912336
67. Das, A., Patel, S. K., & Das, S. R. (2019). Performance comparison of vegetable oil based nanofluids towards machinability improvement in hard turning of HSLA steel using minimum quantity lubrication. *Mechanics & Industry, 20*, 506. https://doi.org/10.1051/meca/2019036
68. Cai, L., Feng, Y., & Liang, S. Y. (2024). Analytical modelling of cutting force in end-milling with minimum quantity lubrication. *International Journal of Precision Engineering and Manufacturing, 25*, 899–912. https://doi.org/10.1007/s12541-023-00837-0
69. Storchak, M., Drewle, K., Menze, C., Stehle, T., & Möhring, H.-C. (2022). Determination of the tool-chip contact length for the cutting processes. *Materials, 15*, 3264. https://doi.org/10.3390/ma15093264
70. Çelebi, C., Özlü, E., & Budak, E. (2013). Modeling and experimental investigation of edge hone and flank contact effects in metal cutting. *Procedia CIRP, 8*, 194–199. https://doi.org/10.1016/j.procir.2013.06.088
71. Bagherzadeh, A., Kuram, E., & Budak, E. (2021). Experimental evaluation of eco-friendly hybrid cooling methods in slot milling of titanium alloy. *Journal of Cleaner Production, 289*, 125817. https://doi.org/10.1016/j.jclepro.2021.125817
72. Molinari, A., & Moufki, A. (2008). The Merchant's model of orthogonal cutting revisited: A new insight into the modeling of chip formation. *International Journal of Mechanical Sciences, 50*(2), 124–131. https://doi.org/10.1016/j.ijmecsci.2007.07.015
73. Shi, T., & Ramalingam, S. (1993). Modeling chip formation with grooved tools. *International Journal of Mechanical Sciences, 35*(9), 741–756. https://doi.org/10.1016/0020-7403(93)90022-M
74. Uysal, A. (2018). Effects of nano graphene particles on surface roughness and cutting temperature during MQL milling of AISI 430 stainless steel. *Materials Testing, 60*(5), 533–537. https://doi.org/10.3139/120.111184
75. Abrão, B. S., Pereira, M. F., da Silva, L. R. R., Machado, Á. R., Gelamo, R. V., de Freitas, F. M. C., Mia, M., & da Silva, R. B. (2021). Improvements of the MQL cooling-lubrication condition by the addition of multilayer graphene platelets in peripheral grinding of SAE 52100 steel. *Lubricants, 9*, 79. https://doi.org/10.3390/lubricants9080079
76. Reeves, C. J., Menezes, P. L., Lovell, M. R., & Jen, T.-C. (2013). The size effect of boron nitride particles on the tribological performance of biolubricants for energy conservation and sustainability. *Tribology Letters, 51*, 437–452. https://doi.org/10.1007/s11249-013-0182-2
77. Devotta, A., Beno, T., Löf, R., & Espes, E. (2015). Quantitative characterization of chip morphology using computed tomography in orthogonal turning process. *Procedia CIRP, 33*, 299–304. https://doi.org/10.1016/j.procir.2015.06.053
78. Ozlu, B. (2021). Investigation of the effect of cutting parameters on cutting force, surface roughness and chip shape in turning of Sleipner cold work tool steel. *Journal of the Faculty of Engineering and Architecture of Gazi University, 36*(3), 1241–1251.
79. Singh, B. K., Roy, H., Mondal, B., Roy, S. S., & Mandal, N. (2019). Measurement of chip morphology and multi criteria optimization of turning parameters for machining of AISI 4340 steel

using Y-ZTA cutting insert. *Measurement, 142*, 181–194. https://doi.org/10.1016/j.measurement.2019.04.064
80. Shah, R., Shirvani, K. A., Przyborowski, A., Pai, N., & Mosleh, M. (2022). Role of nanofluid minimum quantity lubrication (NMQL) in machining application. *Lubricants, 10*, 266. https://doi.org/10.3390/lubricants10100266
81. Sun, J., Huang, Z., Zhao, J., & Yan, K. (2021). Nano-laminated graphene-carbide for green machining. *Journal of Cleaner Production, 293*, 6158. https://doi.org/10.1016/j.jclepro.2021.126158
82. Demir, U., Yapan, Y. F., Uslu Uysal, M., & Uysal, A. (2023). Sustainability assessment and optimization for milling of compacted graphite iron using hybrid nanofluid assisted minimum quantity lubrication method. *Sustainable Materials and Technologies, 38*, e00756. https://doi.org/10.1016/j.susmat.2023.e00756
83. Yang, H., Wu, J., Chen, F., Guo, Z., Xue, X., Chen, Y., & Xu, G. (2023). Life cycle climate performance evaluation of electric vehicle thermal management system under Chinese climate and driving condition. *Applied Thermal Engineering, 228*, 120460. https://doi.org/10.1016/j.applthermaleng.2023.120460
84. Khan, A. M., Gupta, M., Hegab, H., Jamil, M., Mia, M., He, N., Song, Q., Liu, Z., & Pruncu, C. I. (2020). Energy-based cost integrated modelling and sustainability assessment of Al-GnP hybrid nanofluid assisted turning of AISI52100 steel. *Journal of Cleaner Production, 257*, 120502. https://doi.org/10.1016/j.jclepro.2020.120502
85. Kim, H.-J., McMillan, C., Keoleian, G. A., & Skerlos, S. J. (2010). Greenhouse gas emissions payback for lightweighted vehicles using aluminum and high-strength steel. *Journal of Industrial Ecology, 14*, 929–946. https://doi.org/10.1111/j.1530-9290.2010.00283.x
86. Priarone, P. C., Ingarao, G., Settineri, L., & Lorenzo, R. D. (2016). On the impact of recycling strategies on energy demand and CO_2 emissions when manufacturing Al-based components. *Procedia CIRP, 48*, 194–199. https://doi.org/10.1016/j.procir.2016.03.044
87. Li, C., Tang, Y., Cui, L., & Li, P. (2015). A quantitative approach to analyze carbon emissions of CNC-based machining systems. *Journal of Intelligent Manufacturing, 26*, 911–922. https://doi.org/10.1007/s10845-013-0812-4
88. El-Hossainy, T. M., El-Tamimi, A. M., & Abdelmaguid, T. F. (2012). Using NSGA-II to optimise tool life and production time for turning under Minimum Quantity Lubrication. *International Journal of Manufacturing Research, 7*(3), 290–310. https://doi.org/10.1504/IJMR.2012.048698
89. Saatçi, E., Yapan, Y. F., Uslu Uysal, M., & Uysal, A. (2023). Orthogonal turning of AISI 310S austenitic stainless steel under hybrid nanofluid-assisted MQL and a sustainability optimization using NSGA-II and TOPSIS. *Sustainable Materials and Technologies, 36*, e00628. https://doi.org/10.1016/j.susmat.2023.e00628
90. Astakhov, V., & Davim, J. P. (2008). *Tools (geometry and material) and tool wear, machining, fundamentals and recent advances* (pp. 29–57). London: Springer.
91. Uysal, A., & Jawahir, I. S. (2021). Optimization of sustainable machining of Ti6Al4V alloy using genetic algorithm for minimized carbon emissions and machining costs, and maximized energy efficiency and human health benefits. In *Proceedings of the ASME 2021 International Mechanical Engineering Congress and Exposition. Volume 2B: Advanced Manufacturing. Virtual, Online*. November, ASME (pp. 1–5). V02BT02A061. https://doi.org/10.1115/IMECE2021-72995
92. Kumar, R., Soni, G., & Chhabra, S. (2013). Optimization of process parameters during CNC turning by using AHP & VIKOR method. *International Journal of Engineering Research & Technology, 2*(12), 3478–3480.
93. Sarina, Zhang, S., & Xu, J. (2013). Transmission system accuracy optimum allocation for multiaxis machine tools' scheme design. *Proceedings of the Institution of Mechanical Engineers, Part C: Journal of Mechanical Engineering Science, 227*(12), 2762–2779. https://doi.org/10.1177/0954406213479723
94. Sim, B., & Lee, W. (2023). Digital twin based machining condition optimization for CNC machining center. *International Journal of Precision Engineering and Manufacturing-Smart Technology, 1*(2), 115–123. https://doi.org/10.57062/ijpem-st.2023.0010

Publisher's Note Springer Nature remains neutral with regard to jurisdictional claims in published maps and institutional affiliations.

Yusuf Furkan Yapan is a research assistant at Yildiz Technical University, Department of Mechanical Engineering. He also continues his on-site doctoral education in this department.

Kerim Türkeli completed his undergraduate education in Mechanical Engineering at Yıldız Technical University.

Uğur Emiroğlu is a lecturer at Kastamonu University, Department of Motor Vehicles and Transportation Technologies, conducting studies on machine tools.

Erkan Bahçe is an associate professor at Inonu University, Department of Mechanical Engineering, conducting studies on machining science.

Alper Uysal is a professor at Yıldız Technical University, Department of Mechanical Engineering, conducting studies on sustainable machining.